Molybdenum burial mechanism in sulfidic sediments: Iron-Sulfide pathway

Trent Vorlicek, George Rudolph Helz, Anthony Chappaz, Pakou Vue, Austin Vezina, and Wayland Hunter

ACS Earth Space Chem., **Just Accepted Manuscript** • DOI: 10.1021/acsearthspacechem.8b00016 • Publication Date (Web): 20 Mar 2018

Molybdenum burial mechanism in sulfidic sediments: Iron-Sulfide pathway

Trent P. Vorlicek[1*], George R. Helz[2], Anthony Chappaz[3], Pakou Vue[1], Austin Vezina[1], Wayland Hunter[1]

[1]Department of Chemistry and Geology, Minnesota State University, Mankato, MN 56001, USA

[2]Department of Chemistry and Biochemistry, University of Maryland, College Park, MD 20742, USA

[3]Department of Earth and Atmospheric Sciences, Central Michigan University, Mount Pleasant, MI 48859, USA

* Corresponding author. Tel.: 507-389-1598

E-mail address: trenton.vorlicek@mnsu.edu

ABSTRACT: Relative to continental crust, sediments underlying sulfidic marine waters are molybdenum-rich, a property preserved in the rock record and useful for characterizing paleoenvironments. The enrichment mechanism is not agreed upon, but is attributed at least partly to deposition of Fe-Mo-S compounds, which are as yet uncharacterized. Here, we determine the composition and stability of colloidal Fe-Mo-S precipitates formed at mildly basic pH and $H_2S(aq)$ > 10^{-5} M. The first product consists simply of $FeMoS_4$, with $K_{sp} = 10^{-14.95}$. Within hours, $FeMoS_4$ irreversibly transforms by internal self-reduction to a Mo(IV) product of similar composition. The reduced product is insoluble in 1 M HCl but soluble in concentrated HNO_3, implying that it would be recovered with pyrite in a common assay of sediments. XAFS data show that Mo(IV) in the colloids is coordinated by a split first shell of about five sulfur atoms at average distances of 2.31 and 2.46 Å and in its second shell by an iron atom at about 2.80 Å. These properties resemble those determined for Mo in modern anoxic lake sediments and in Phanerozoic black shales. The atomic environment around Mo suggests that the colloidal products may be inorganic polymers containing cuboid, $Fe_2Mo_2S_4^{4+}$ cores. Such materials are so far unreported by mineralogists, although a rare mineral, jordisite, may be a related, but more Mo-rich material. The low solubility of $FeMoS_4$ makes it a feasible precipitate in euxinic waters like those in the modern Black Sea. We propose that colloids similar to those studied here could account for Mo-enrichment in euxinic basin sediments and black shales.

Keywords: Molybdenum, euxinic basins, iron sulfide, jordisite, colloids

1. INTRODUCTION

Molybdenum (Mo) concentrations in ancient black shales and modern sediments shed light on the redox state of Earth's ocean-atmosphere system and on recent anoxic events in marine basins.[1,2] Molybdenum serves as a paleo-redox proxy for past sulfidic conditions because its concentrations in black shales increase from detritic background (1-2 ppm) to exceptionally high values (up to 200-300 ppm) when redox conditions shift from oxic to euxinic.[3,4] Two pathways are being considered to explain Mo sequestration under euxinic conditions:[5,6] (1) the iron-sulfide pathway[7-10] and (2) organic matter pathway.[6,11,12] Quantitative tests of these pathways are not possible at present. The goal of this paper is to put the first on a quantitative footing.

The idea that Mo in euxinic basins follows an iron-sulfide pathway has a long history.[13-17] Modern support for this pathway comes from X-ray Absorption Fine Structure (XAFS) studies: S atoms are found in the first coordination shell and Fe atoms in the second coordination shell around Mo atoms in some black shales and anoxic lake sediments.[7,18,19] Based on field data from Rogoznica Lake,[8] a quantitative thermodynamic model of Mo deposition in sulfidic waters via an iron sulfide pathway was proposed. The model postulated existence of an unknown mineral with an approximate, empirical formula, $FeMo_{0.6}S_{2.8}$. This model predicted water-column Mo concentrations in a half-dozen euxinic water bodies to within about a factor of three. In *post facto* tests, it predicted Mo concentrations in the sulfidic water column of Green Lake and in the sulfidic pore waters of Terrebonne Bay sediments to a similar level of accuracy.[20,21] Nevertheless, a weakness of this model is that compounds approaching the proposed mineral composition are unknown to both mineralogists and inorganic chemists. Possibly this material has evaded discovery in nature because its structure is unsuited to ordered crystallization, and therefore it is necessarily colloidal and x-ray amorphous.[8]

Evidence has accumulated over several decades that suspended FeS particles, often of colloidal size, are commonly found in sulfidic waters.[22-30] In this paper, we determine properties of

Fe-Mo-S precipitates formed by the reaction of colloidal FeS with thiomolybdate, and we propose that products of this reaction are significant Mo hosts in sediments of euxinic basins.

2. METHODS

Materials. The following reagents were purchased and used as received: $Na_2B_4O_7{\cdot}10H_20$ (Sigma-Aldrich), orthorhombic sulfur (Sigma-Aldrich), $Fe(NH_4)_2(SO_4)_2{\cdot}6H_2O$ (Mallinckrodt), $MgCl_2{\cdot}6H_2O$ (BDH), $HgCl_2$ (J.T. Baker), Na_2O_2 (Merck), $BaCl_2{\cdot}2H_2O$ (Fisher), Na_2SO_4 (Mallinckrodt), Na_2CO_3 (Fisher), 0.1000(±0.0001) M EDTA (Alfa-Aesar), LC-MS grade acetonitrile (EMS), and tetrabutylammonium hydroxide thirty hydrate (Sigma). $Na_2S{\cdot}9H_2O$ (Sigma-Aldrich) crystals were individually rinsed with H_2O until any yellowish oxidative impurities were no longer visible.

Several authors have noted that commercial $(NH_4)_2MoS_4$ reagents often contain substantial amounts of an unidentified impurity, giving them a mauve-brown color rather than their normal deep red color, which is like that of a full-bodied red wine.[31,32] The specific impurity has not been identified, but it may be a dimeric Mo(V)-polysulfido compound (e.g., $(NH_4)_2Mo_2O_2(\mu\text{-}S)_2(S_2)_2$), arising from oxidation over long storage times.[33] Consequently, we opted to avoid commercial thiomolybdate reagents, instead synthesizing fresh $(NH_4)_2MoS_4$ by the reaction of MoO_4^{2-} with sulfide.

Test Solution Procedures. Solutions were prepared at room temperature using deoxygenated ultrapure H_2O in an anaerobic chamber under a 95% N_2:5% H_2 atmosphere. $Na_2B_4O_7{\cdot}10H_2O$ and $Na_2S{\cdot}9H_2O$ were placed into a 1 L beaker. Following addition of ~800 mL of H_2O, the pH was adjusted, and an aliquot of MoS_4^{2-} stock solution previously standardized by UV-vis absorbance[34] was added. After diluting to 1L, the required volume of Fe^{2+} stock solution was added, resulting in formation of a stable, inky-black, colloidal suspension. Fourteen mL of this suspension was apportioned into each of a series of 15 mL plastic centrifuge tubes that were then capped and stored in the glove box. Upon aging ~100 hours, centrifuge tubes were opened within the glovebox and 350 μL of 4 M $MgCl_2$ was added to promote flocculation of the colloids; tubes

were again capped and stored in the glovebox. Flocculation was unsatisfactory unless $MgCl_2$ was added after some aging.

Analyses. At various times, individual centrifuge tubes were opened and their contents filtered through Whatman 0.02 μm syringe filters. Filtered aliquots were immediately passed out of the anaerobic chamber for UV-vis analyses (Schimadzu UV-2450 double-beam spectrophotometer). We calculated MoS_4^{2-} concentrations using extinction coefficients,[35,36] attributing all absorption at 468 nm to MoS_4^{2-}. Samples were treated with BrCl to oxidize sulfide and with aluminum (1000 ppm) as a matrix modifier prior to determination of total dissolved Mo by atomic absorption spectroscopy (Perkin-Elmer PinAAcle 900T spectrophotometer).

At the end of a run, three samples were analyzed separately to obtain average total sulfide and pH. Total sulfide was titrated with standardized Hg^{2+} to a potentiometric endpoint (Ag/Ag_2S vs. double junction reference electrodes) after adjusting the solution to pH ~13. This titration quantifies the sum of H_2S and HS^- plus any sulfide ligands associated with thiomolybdates and dissolved Fe-Mo-S complexes. Free sulfide (H_2S+HS^-) was calculated from the titration result after subtracting four times the measured MoS_4^{2-} concentration and five times the excess of ΣMo over MoS_4^{2-}. Under the experimental conditions, this excess is due mostly to dissolved $[(FeS)_2(MoS_4)_2]^{4-}$.

Precipitate characterization. Precipitates used in the solid-phase analyses were obtained by filtering test solutions with 47 mm diameter, 0.45 μm pore size Tuffryn® or Metricel® membrane filters (Pall Life Sciences). The filtered solids were washed with several ~50 mL portions of ultrapure H_2O and dried in the anaerobic chamber. The filter with filtrand was stored in the anaerobic chamber until analysis.

Precipitates were freeze-dried prior to x-ray diffractometry (Rigaku Ultima-4 X-ray diffractometer, Cu Kα radiation, excitation energy 40 kV and 44 mA, scan rate 5°/min, step size 0.01°). Energy dispersive spectroscopy was performed on a ~0.5 cm^2 piece of filter fixed to a nylon

stub with carbon tape (Jeol 6510 LV scanning electron microscope equipped with a Thermo-Noran EDS System 7 and a Thermo-Noran Silicon Drift Detector; 20 kV accelerating voltage; 16 mm working distance; 0.066 μm spot size). More than 20,000 counts were obtained at each spot, implying counting errors of 1% or less; about 95 spots were assayed per sample.

Peroxide digestion was used for elemental analyses. Precipitates were resuspended from filters by immersing the filters in water and shaking. The filters were removed and the water evaporated to dryness. Between 10 and 15 mg of dried precipitate was placed in a 50 mL Ni crucible with about 80 to 120 mg Na_2O_2. After capping the crucible, its contents were fused gingerly for 20 minutes over an air-CH_4 flame. Upon cooling, the products in the crucible were leached with water, which was then filtered (0.45 μm Metricel® membrane filters). The filtrands were dissolved into 0.1 M HCl and analyzed by atomic absorption spectroscopy (Fe, Mo, Mg). Filtrate solutions were analyzed using reverse-phase ion pair chromatography (IPC: SO_4^{2-}, MoO_4^{2-}; Dionex IonPac NS1, conductivity detection). As a check, sulfate was also quantified turbidimetrically. Additional details concerning the turbidimetric and IPC methods are found in Supporting Information.

X-ray Absorption Fine Structure spectroscopy was performed at beamline 13-BM-D at the Advanced Photon Source, Argonne National Laboratory. Powdered precipitates were packed into Teflon sample holders that were then sealed with Kapton tape within a glove box containing N_2 atmosphere. During data collection, a constant flux of He was injected in a plastic bag containing our sample holders to prevent any oxidation. A Si (111) double crystal monochromator was used in conjunction with harmonic rejection mirrors. Fluorescence X-rays were measured using a Canberra 16 element Ge detector. The incident beam intensity was detuned by ~20–30% to reject higher-order harmonic frequencies. Spectra were collected with energy and wave number resolution prior to the edge (19,850–19,980 eV); across the Mo K-edge (19,980–20,050 eV); and throughout the EXAFS region (20,050–20,700 eV) at 4 eV, 0.3 eV, and 0.05Å−1Å, respectively. At least three

spectra per sample were merged to improve the signal-to-noise ratio and resolution. Energy calibration was maintained by simultaneous measurements of a Mo(0) foil in transmission mode as an internal standard. The first and fourth peaks in the first derivative of the Mo(0) foil were assigned 20,000.0 and 20,039.1 eV. For data interpretation, five Mo standards were also characterized: $Mo(IV)O_2(s)$, $Mo(IV)S_2(s)$, $Mo(VI)O_3(s)$, $Mo(VI)O_4^{2-}(aq)$, and $Mo(VI)S_4^{2-}(aq)$. All data were processed and analyzed using the Demeter software package.[37]

Two features from the XANES region are particularly useful for delineating differences between Mo compounds: the pre-edge features (i.e. the presence, amplitude, and position of a peak before the edge) and the maximum peak (*Em*). A pronounced pre-edge feature is characteristic of terminal Mo=O double bonds (MoO_4^{2-}) and an octahedral configuration. This pre-edge feature is less pronounced for Mo=S double bonds (MoS_4^{2-}) and absent when only single bonds are present (i.e. $MoO_{2(s)}$ and $MoS_{2(s)}$). *Em* increases with the Mo oxidation state.[18,19]

Thermodynamic Model. We calculated speciation in the solutions by solving the following mass balance equation for dissolved Fe:

$$\Sigma Fe = Fe^{2+} + FeOH^{+} + FeCl^{+} + Fe(HS)_2^0 + [FeO(OH)MoS_4]^{3-} + 2[(Fe_2S_2)(MoS_4)_2]^{4-} \quad (1)$$

Iron sulfide cluster complexes were excluded from this equation in the light of recent findings.[38,39] Assuming chemical equilibrium, this equation can be solved for Fe^{2+} by replacing the term for each species by an expression that includes an analytically determined ligand concentration and a stability constant obtained from published sources.[9,40,41] Activity coefficients were evaluated by the Davies equation. When Fe^{2+} had been calculated, the concentrations of all complexes then could be obtained by back substitution into the equilibrium constant expressions.

In solving equation 1, the measured total Mo concentrations were not used. Therefore, the validity of this thermodynamic model could be tested by comparing the sum of calculated Mo species concentrations against the measured total Mo. Results of this test are shown in Figure 1, which reveals excellent agreement between measured and calculated values except for a small

departure in the sample having the highest Mo concentration. This agreement verifies the model and the choices of stability constants, as well as the implicit assumption that all dissolved *but not precipitated* Mo is in the +VI oxidation state.

3. RESULTS

Precipitate Formation. Table 1 summarizes both initial and final Mo, Fe and ΣS(-II) concentrations for all runs. Figure 2 shows a representative time course for an experiment. At mildly alkaline pH, no precipitation occurs from a solution containing only thiomolybdates and sulfide, but a stable colloidal suspension forms as soon as Fe(II) is added. The inset graph in Figure 2 compares optical absorption by the solution before and after colloids were flocculated with 0.1 M $MgCl_2$ and removed by filtration. Prior to $MgCl_2$ introduction, MoS_4^{2-} can be quantified by intense absorption peaks at 318 and 468 nm, but colloids must be flocculated and removed in order to quantify dissolved Mo, Fe, and sulfide.

The initially-formed colloids are likely to consist mainly of iron sulfide, which precipitates rapidly.[42] The high $\Sigma S^{-II}/\Sigma Fe^{II}$ ratios and neutral pH of our solutions inhibit mackinawite crystal growth,[43] preserving colloidal FeS in an unstable state as it reacts slowly with MoS_4^{2-} (Figure 2). About half of the total MoS_4^{2-} losses occur in the first day, but losses continue for many days. To allow precipitation to reach completion, we aged precipitates for 300 to 4000 h (4th column, Table 1), but we found no analytically significant trends with aging beyond 300 h.

Curiously, the visual appearance of flocculated particles differed in solutions with high vs. low initial Fe/Mo mole ratios ($N_{Fe/Mo}$). At initial $N_{Fe/Mo}>1$, flocculated particles are large, wispy black sheets that settle appreciably within ~20 minutes after $MgCl_2$ addition. In contrast, flocculated particles in solutions with initial $N_{Fe/Mo}<1$ are barely visible black clumps after 2 days of exposure to $MgCl_2$ and mostly remain suspended until captured by filtration. These qualitative observations hint that the phase composition of the precipitates differs depending on initial $N_{Fe/Mo}$.

Figure 3 shows some experiments to test reversibility after various aging times by spiking $MgCl_2$-free aliquots of colloidal suspensions with EDTA to a concentration of 10^{-3} M, which is in substantial excess to the total Fe (precipitated + dissolved). We established that this complexing agent has no effect on the optical absorbance of MoS_4^{2-}. However it drops the activity of Fe^{2+} by a factor of $>10^4$, causing a resurgence of dissolved MoS_4^{2-} absorbance from fresh precipitates. On the other hand, after only a few hours of aging, the figure shows that precipitates no longer release most of their MoS_4^{2-}. Apparently, aging transforms the precipitates to much less soluble secondary products in this time period. Nevertheless, a few percent of precipitated MoS_4^{2-} remain in an EDTA-reactive state, possibly as surface layers on the colloidal particles.

Solution composition. At the pH and sulfide concentrations of these runs, optical absorption showed that MoS_4^{2-} was overwhelmingly the predominant ion in the $MoO_nS_{4-n}^{2-}$ (n = 0 to 4) series, as anticipated from thermodynamics.[34] Table 2 presents concentrations of selected other species obtained from the thermodynamic model. The fourth and fifth columns give the concentrations of the two most abundant Fe and Fe-Mo complexes. Not shown are the minor species that were considered ($FeOH^+$, $FeCl^+$ and $[FeO(OH)MoS_4]^{3-}$), but the sixth column shows the sum of Mo concentrations in all dissolved species in each run. This sum was plotted against the measured total Mo concentration in Figure 1 to verify the thermodynamic model.

The last two columns in Table 2 list logarithms of activity products, Q_{FeS} and Q_{MoS3}, which we define as:

$$Q_{FeS} = \{Fe^{2+}\}\{H_2S\} / 10^{-2pH} \quad (2)$$

$$Q_{MoS3} = \{MoS_4^{2-}\}\ 10^{-2pH} / \{H_2S\} \quad (3)$$

(In this paper, braces denote activities of dissolved species; Q designates any activity product whereas K designates an activity product *at equilibrium with a solid phase*.) The Q values are proportional to the activities of FeS and MoS_3 components (a component being one of the minimum number of independently variable constituents required to specify the composition of a phase). For

example, we can write $a_{FeS} = Q_{FeS}/C_s$ where the constant of proportionality, C_s, defines the standard state and thus the a_{FeS} scale. If we preferred to designate pure mackinawite (tetragonal FeS) as having $a_{FeS} = 1$, then C_s would be equated to mackinawite's conventional solubility product constant ($K_{mack} = 10^{3.21}$ at 25°C).[44] If, on the other hand, we wished to designate nanocrystalline FeS as having $a_{FeS} = 1$, then C_s would be $K_{FeSam} = 10^{4.87}$.[45] No choice of standard state is more correct than another, and for simplicity we will let C_s be unity, thus employing the Q values themselves as measures of the activities of their respective components. (In this case, the standard states for a_{FeS} and a_{MoS3} are ideal aqueous solutions in which the component ions are present at unit concentrations.)

In Figure 4, log Q_{MoS3} has been plotted against log Q_{FeS}. The excellent inverse correlation reveals that the activities of FeS and MoS_3 are linked by a solubility equilibrium. The Gibbs-Duhem equation specifies that the slope in this kind of plot is equal to minus the molar Fe/Mo ratio in the precipitate. Because log Q_{FeS} and log Q_{MoS3} are linearly correlated, with an approximate slope of -1 (actual error-weighted regression value -0.94 ± 0.11, R^2 0.95), we infer that over the > 2 log unit range of log Q_{FeS} in these experiments, the phase with which the solutions have equilibrated possesses a fixed composition with Fe/Mo = 1. Thus, the phase must be $FeMoS_4$. If this phase were a solid solution having a significant range in Fe/Mo ratio, then the data in Figure 4 would display a non-linear trend.

Employing the regression equation in Figure 4 and the definitions in equations (2) and (3), the solubility product constant of this $FeMoS_4$ precipitate is given by:

$$K_{FeMoS4} = (Q_{MoS3})(Q_{FeS}) = \{Fe^{2+}\}\{MoS_4^{2-}\} = 10^{-14.95 \pm 0.06} \quad (4)$$

The standard free energy of formation from its elements of this colloidal precipitate is $\Delta G_f^0 =$ −1227.2 kJ/mol. For comparison, published data indicate that the corresponding solubility product for $FeMoO_4$ is $10^{-10.48}$ and $\Delta G_f^0 = -975$ kJ/mol.[46] The large difference in solubility shows why converting MoO_4^{2-} to MoS_4^{2-} in sulfidic waters initiates Mo precipitation. The stability constant

and ΔG_f^0 values derived here refer to $FeMoS_4$, not the secondary product formed after a few hours of aging. Because the secondary product has formed irreversibly, we can learn nothing of its stability from measurements of solution composition.

Precipitate Properties. Figure 5 presents x-ray diffraction patterns for precipitates obtained at three initial Fe/Mo mole ratios. With no Mo in the initial solution (top trace), the pattern is similar to that of nanoparticulate FeS.[47,48] The most prominent peaks of crystalline mackinawite can be recognized, but they are broadened and shifted to smaller 2θ (larger interplanar distances). In the absence of added Mo, these effects must be attributed to small particle size and the resulting lattice relaxation. Adding a small amount of MoS_4^{2-} to the initial solution (middle trace) dilutes the mackinawite peaks and adding MoS_4^{2-} in excess to Fe^{2+} (bottom trace) largely erases them. Significantly, no new peaks are created. Evidence for weak mackinawite peaks in the bottom trace may be due to survival of a small amount of mackinawite in cores of what are otherwise amorphous particles.

As shown in Figure 6, we also characterized compositions of several precipitates by energy dispersive spectroscopy. The panels depict experiments that are arranged according to the ratio of initial Fe to initial Mo with the most Fe-rich experiment at the top. The horizontal axes in this figure are the ratios of counts obtained for the Fe peak at 6.40 keV to the sum of counts for Fe plus the counts for overlapping Mo and S peaks at ~2.30 keV. Overlap prevented obtaining independent Mo and S counts and, thus, quantifying elemental ratios.

The precipitate in the top panel contains solely iron sulfide. The observed dispersion in count ratios probably is indicative of the instrument's energy resolution with colloidal particles. In panels b and c, where Mo is present but the amount is not sufficient to convert all the FeS to $FeMoS_4$, the observed dispersion in count ratios is much larger than in panel a. Apparently, the precipitate is chemically heterogeneous, and the electron beam is encountering the FeS and $FeMoS_4$ phases in varying proportions as different spots are sampled. This evidence implies that the

precipitates consist of discrete phases, not a homogeneous solid solution phase, but does not exclude limited Fe/Mo variation within either phase. In panels d and e, where enough Mo relative to Fe is initially available to convert all FeS to $FeMoS_4$, the dispersion in precipitate compositions again resembles that in panel a, suggesting that a single $FeMoS_4$ phase is present. Nevertheless, further increase in initial Mo produces a new phase still richer in Mo (panel f).

Figure 7 presents XANES spectra for several standards as well as for precipitates generated by runs 6, 7, 9 and 12. A pre-edge peak near 20005 eV is seen in the standards containing Mo(VI) but is absent from the standards containing Mo(IV). This peak is also absent from the spectra of all precipitates. Additionally, the precipitates' maximum absorption energies (E_m) are similar to those for Mo(IV) standards (Figure 7 and Table 3). These features provide evidence that Mo has been reduced. Additionally, fits to EXAFS spectra (Table 4) indicate that the first two coordination shells around Mo are occupied by approximately 2 and 3 sulfur atoms at distances of 2.30 – 2.32 Å and 2.44 – 2.47 Å, respectively. These interatomic distances are clearly longer than interatomic distances for MoS_4^{2-} (2.18 Å). If we consider the average of the shorter Mo–S interatomic distance for our precipitate (2.31 Å), it is similar to data for the type S sediment samples from Lake Cadagno (2.26–2.38 Å).[18] The longer Mo-S distances were not observed in Cadagno, possibly because of greater disorder. When the Lake Cadagno EXAFS modeling was run, only one type of Mo–S bond was considered and tested for EXAFS modeling. The EXAFS evidence rules out $MoS_{2(S)}$, $MoS_{3(S)}$ and MoS_4^{2-} as major constituents in the aged precipitates. Modeling of the third shell reveals that Mo is bound to an Fe atom at a distance of 2.79–2.81 Å. These Mo–Fe interatomic distances, although longer, remain comparable to those determined in Lake Cadagno type S samples (2.71–2.73 Å). These comparisons suggest that the precipitates are structurally similar to products found in natural euxinic environments.

Huerta-Diaz and Morse found that Mo was not appreciably dissolved from modern sulfidic sediments by 1 M HCl but was dissolved to a large extent by concentrated HNO_3[17] an oxidizing

acid. They interpreted this finding as evidence that Mo was mainly hosted by pyrite, which requires concentrated HNO_3 for dissolution. We applied this test to a precipitate that formed under conditions of Run 1. Wet precipitate was placed in each of two centrifuge tubes. Air-saturated, 1 M HCl was added to one and concentrated HNO_3 to the other. Visible solid disappeared immediately in HNO_3, but persisted in HCl for >250 days; AAS analyses confirmed that only the HNO_3 solution had appreciably dissolved Mo. This result implies that oxidation is required to dissolve the Mo(IV) contained in aged Fe-Mo-S precipitates. It also weakens support for the inference of Huerta-Diaz and Morse that Mo is hosted mainly by pyrite in modern sulfidic sediments.

Because sulfidic sediments exposed to NaOH have been shown to leach a significant portion of particle-bound Mo, [50] workers have concluded that Mo must be hosted by humic materials. As a test, we added 1 M NaOH to a precipitate formed under the conditions of Run 6. After filtering, AAS analyses of the filtrate showed that >20% of Mo initially present in the precipitate had dissolved. These results imply that leaching of Mo by NaOH can not be used on its own as evidence of organic-bound Mo in sulfidic sediments.

Sulfide as reductant. Reduction of Mo(VI) in solution to Mo(IV) in precipitates requires a reducing agent, which in these experiments can only be sulfide. The electron transfer could be internal, between Mo(VI) and coordinating S(-II) atoms, or external, between HS^-(aq) and $FeMoS_4$(s). These options can be represented as:

$$FeMoS_4(s) \rightarrow FeMoS_2(S_2)(s) \quad (5)$$

$$FeMoS_4(s) + {}^{1}/_{(n-1)}\, HS^- \rightarrow FeMoS_3(s) + {}^{1}/_{(n-1)}\, S_n^{2-} + {}^{1}/_{(n-1)}\, H^+ \quad (6)$$

where (S_2) represents a disulfide ligand in the precipitate structure and S_n^{2-} represents a dissolved polysulfide ion.

Molybdenum sulfides that include disulfide ligands are well known. Simply acidifying a MoS_4^{2-} solution rapidly produces dissolved species such as $Mo^{V}_2S_4(S_2)_2^{2-}$.[51] Even amorphous $MoS_{3(s)}$, which is nominally a Mo(VI) compound, is known actually to be $Mo^{IV}S(S_2)$.[52-54]

We approached the question of whether reaction 5 or 6 best describes the evolution of our precipitates in two ways. First, we looked for optical absorption evidence for dissolved polysulfide ions.[55] This approach was obstructed in most runs by swamping optical absorption from MoS_4^{2-} and $[(FeS)_2(MoS_4)_2]^{4-}$. Only in one case, run 16, was interference from these sources low enough to obtain the concentration of dissolved S(0) in polysulfides. The result was about ⅓ mole dissolved S(0) per mole Mo precipitated, implying that at least ⅔ mole S(0) per mole Mo was retained by the precipitate. Retention could be higher if some O_2 contamination were responsible for the dissolved S(0) that was observed. Second, we analyzed several aged precipitates. From three solutions initially containing $N_{Fe/Mo}$ = 0.20, 0.13 and 0.10, we obtained precipitates with empirical formulas of $Fe_{0.78}MoS_{3.83}$, $Fe_{0.83}MoS_{3.75}$ and $Fe_{0.63}MoS_{3.60}$ respectively. These contained very small amounts of Mg^{2+} adsorbed from the electrolyte. Additionally, 45% to 50% of their masses was unexplained and presumed to be water, a common component of flocculated colloids. If all Fe in these formulas has a +2 charge and all molybdenum has a +4 charge (as required by x-ray spectroscopic data), then charge balance requires that anions in these formulas possess a total charge of -5.56, -5.66 and -5.26 respectively. If all of this negative charge is supplied by the sulfur (i.e. none from bound OH^- or Cl^-), then the implied final formulas would be $Fe_{0.78}MoS_{1.73}(S_2)_{1.05}$, $Fe_{0.83}MoS_{1.91}(S_2)_{0.92}$ and $Fe_{0.63}MoS_{1.66}(S_2)_{0.97}$. Apparently, these precipitates have retained about one mole of zero-valent sulfur (contained in S_2^{2-}) per mole of Mo, suggesting that reaction 5 is better than reaction 6 as a representation of the secondary material's formation.

These analyses suggest that precipitates kept in Mo-rich solutions during weeks of aging contain Fe/Mo somewhat smaller than the value of unity inferred for the initial precipitates from Figure 4. Possibly, $FeMoS_4$ takes on additional Mo or loses some Fe as it converts to its aged form.

Alternatively, the recovered products might contain a small amount of the additional, Mo-rich phase revealed by Figure 5f.

4. DISCUSSION

Mo removal from sulfidic natural waters. To optimize experimental control, the precipitates reported here were produced in solutions containing higher Mo and S(-II) concentrations and higher pH than normally found in natural sulfidic waters. Can these precipitates form in nature? In order to investigate this question, we apply a thermodynamic model to the extensive data available for the Black Sea, the largest modern euxinic basin. This evaluation relies on an assumption that dissolved species reach aqueous-phase equilibrium during the centuries that deep water is resident in the Black Sea.

From published analyses and stability constants, we first calculate the following activities in the Black Sea's sulfidic waters: $\{Fe^{2+}\}_{BS}$, $\{H_2S\}_{BS}$ and $\{MoS_4^{2-}\}_{BS}$ (the BS subscript denotes activities in the Black Sea's water). Sources of data and results are presented in Table S1. Then, we compare the $\{MoS_4^{2-}\}_{BS}$ values to $\{MoS_4^{2-}\}_{eq}$ values that would be required for saturation with respect to $FeMoS_4$; $\{MoS_4^{2-}\}_{eq}$ is calculated from a rearrangement of equation 4:

$$\{MoS_4^{2-}\}_{eq} = \frac{10^{-14.95}}{\{Fe^{2+}\}} = \frac{10^{-14.95}\{H_2S\}}{(Q_{FeS})10^{-2pH}} \quad (7$$

If precipitation of $FeMoS_4$ controls total Mo in the Black Sea, $\{MoS_4^{2-}\}_{BS}$ should be approximately equal to $\{MoS_4^{2-}\}_{eq}$. It will not matter that $FeMoS_4$ in the Black Sea would soon transform irreversibly to $FeMoS_2(S_2)$. In an analogous situation, labile FeS phases control dissolved Fe in sulfidic waters even though these phases are transforming irreversibly to FeS_2.

Figure 8 presents the results of this assessment. At the time when the Black Sea was sampled, sulfide concentrations exceeding 1 μM appeared below a suboxic-to-anoxic transition at 90 m depth. Panel A shows that with increasing depth, the hydrogen sulfide activity, $\{H_2S\}_{BS}$, rose continuously all the way to the bottom. Although $\{Fe^{2+}\}_{BS}$ rose with increasing depth in the uppermost sulfidic waters, owing to reductive dissolution of Fe^{III} in sinking particles, this trend

reversed below 150 m. The likely reason is that the water became saturated with FeS, forcing $\{Fe^{2+}\}$ to decline as $\{H_2S\}$ continued to increase. Panel B shows that total dissolved Mo in the uppermost sulfidic water column changed negligibly with respect to overlying oxic and suboxic waters, but it began to decline below about 150 m. In Panel C, the solid red triangles show that despite negligible variation in total dissolved Mo above 150 m, $\{MoS_4^{2-}\}_{BS}$ rose sharply in this region; this was due to conversion of MoO_4^{2-} to MoS_4^{2-}. In contrast, below 150 m, the figure shows that $\{MoS_4^{2-}\}_{BS}$ ceased to change appreciably even though total dissolved Mo then began to decline very significantly. In this region, any additional MoS_4^{2-} produced by rising sulfide was removed from the water, causing loss of total Mo at nearly constant $\{MoS_4^{2-}\}_{BS}$. Most of the loss of total dissolved Mo from the entire water column occurred in the zone where some removal process was fixing $\{MoS_4^{2-}\}_{BS}$ at nearly constant values. The disconnect between behaviors of total dissolved Mo and $\{MoS_4^{2-}\}_{BS}$ is striking.

Is it plausible that saturation with respect to $FeMoS_4$ is the process that fixed $\{MoS_4^{2-}\}_{BS}$? The answer to this question depends on the values of $\{Fe^{2+}\}_{BS}$, or alternatively, Q_{FeS}. The open diamond symbols in Panel C depict $\{MoS_4^{2-}\}_{eq}$ values obtained from equation 7 by assuming that ambient $\{Fe^{2+}\}_{BS}$ at each depth controlled $\{MoS_4^{2-}\}_{eq}$. The diamond symbols show that $\{MoS_4^{2-}\}_{eq}$ is greater than $\{MoS_4^{2-}\}_{BS}$ by more than two orders of magnitude. Seemingly, the Black Sea is immensely under saturated with respect to $FeMoS_4$. If correct, then $FeMoS_4$ precipitates cannot control dissolved Mo in the Black Sea.

However, this difficulty can be circumvented if the operative $\{Fe^{2+}\}_{BS}$ values are much higher than the ambient values in bulk water. (Bulk water is defined here simply as water in quantities usually taken for analysis.) Perhaps higher $\{Fe^{2+}\}_{BS}$ exists in microenvironments where reductive dissolution of iron is taking place, for example at surfaces of Fe(III)-rich particles, or in pore spaces of composite particles and flocs. Support for this idea can be found by considering FeS. Below 150 m, log Q_{FeS} in bulk water averages 2.60 ± 0.17 (Table S1), which is much smaller

than 3.38 at mackinawite saturation or 4.03 at amorphous FeS saturation.[56] Thus, the deep waters of the Black Sea are also immensely under saturated with respect to FeS, even though FeS and phases derived from it (greigite, pyrite) are known to exist there.[25,28]

Experiments show that nucleation of FeS nanoparticles occurs at log $Q_{FeS} \geq 4.87$, [45] which is 2.3 log units larger than average log Q_{FeS} in the deep Black Sea's bulk water. If we suppose that iron sulfide precursors form in microenvironments where log $Q_{FeS} \geq 4.87$, then $FeMoS_4$ could also form there. This is demonstrated in Figure 8C by open square symbols, which show $\{MoS_4^{2-}\}_{eq}$ values calculated from equation 7 by assuming that log $Q_{FeS} = 4.87$. The resulting $\{MoS_4^{2-}\}_{eq}$ values are in reasonable agreement with $\{MoS_4^{2-}\}_{BS}$ values, fulfilling the feasibility criterion for $FeMoS_4$ control of total dissolved Mo.

If $FeMoS_4$ colloids indeed form on or within Fe(III)-bearing particles, then they would be carried to the sediments with the particles. As $FeMoS_4$ settles aboard its natal particles, it can experience elevated Fe(II) activity only until the Fe(III)-pool has been exhausted. The Fe(II) activity will then decline to ambient levels, dropping log Q_{FeS} to values permissive of $FeMoS_4$ dissolution. How could $FeMoS_4$ persist in these undersaturated waters and ultimately survive as a Mo burial product? In addition to the demonstrated irreversibility of its formation, $FeMoS_4$ dissolution requires strongly oxidizing conditions. Given the persistently euxinic water column of the Black Sea, it is reasonable to assume $FeMoS_4$ could survive to burial within Black Sea sediments.

In euxinic basins like the Black Sea, Mo probably is trapped in sediments permanently as $FeMoS_2(S_2)$ colloids. EXAFS patterns resembling those of $FeMoS_2(S_2)$ colloids have been reported from Phanerozoic black shales.[7] However, in environments subject to seasonal fluctuations between oxic and anoxic conditions, trapped Mo is apt to be partially or fully dissolved by exposure to O_2; rapid oxidation has been demonstrated in resuspension experiments.[57]

Some continental shelf sediments are considerably enriched in Mo even though negligible sulfide is found in the seawater above them. In these environments, Mo is believed to diffuse into the seafloor, where it encounters sulfide.[58,59] Because reduction of Fe(III) is ongoing in these environments,[60] the Mo-fixing mechanism described above is expected to operate in the same manner.

Comparison to synthetic compounds. Clues to the atomic structure of the precipitates can be gleaned from known structures of synthetic Fe-Mo-S compounds by comparing Mo-S and Mo-Fe interatomic distances. The Mo-S distances in Table 4 are conspicuously long and suggestive of cuboid compounds.[61-64] Most Fe-Mo-S cuboids have been prepared in non-aqueous solvents and stabilized by organic ligands, but the cuboidal $[FeMo_3S_4(H_2O)_{10}]^{4+}$ cation illustrated in Figure 9 has been prepared in 2 M aqueous HCl.[65] The interatomic distances in this cation (see caption) are similar to those in our precipitates (Table 4). In contrast, most non-cuboid Fe-Mo-S compounds have substantially shorter Mo-S interatomic distances and slightly longer Mo-Fe distances. For example, the structure of the non-cuboid complex, $[(FeS)_2(MoS_4)_2]^{4-}$, which is the principal dissolved Fe-Mo-S complex in our solutions, has Mo-$S_{\mu 2\ bridge}$ interatomic distances of 2.24Å and Mo-$S_{terminal}$ distances of 2.15Å; Mo-Fe distances are 2.78Å.[66] Comparable distances have been reported for a number of similar, non-cuboidal complexes.[67] Additionally, the formal oxidation state in $[(FeS)_2(MoS_4)_2]^{4-}$ is Mo^{VI}, but is Mo^{IV} in our aged precipitates. These comparisons indicate that $[(FeS)_2(MoS_4)_2]^{4-}$ and similar non-cuboid complexes are poor models for the building blocks of our aged precipitates. They also emphasize the point that Mo in the precipitates is chemically quite distinct from Mo in solution.

Core compositions in known cuboid compounds form a complete series from Fe_4S_4 to Mo_4S_4.[64] If we double the inferred empirical formula for our secondary product (reaction 5), the result is $Fe_2Mo_2S_4(S_2)_2$. This suggests that our precipitates might have $[Fe_2Mo_2S_4]^{4+}$ cores coordinated at the Mo positions by disulfide ligands (illustrated in Figure 9). On the other hand,

panel f of Figure 5 hints that initial solutions having very low $N_{Fe/Mo}$ ratios produce precipitates that are much less Fe-rich, possibly containing $FeMo_3S_4$ or even Mo_4S_4 cores. From solutions having extremely low initial $N_{Fe/Mo}$, precipitates with less than 1 mol % Fe have been obtained,[11] but only in the presence of microbial cells or their non-living degradation products. The chemical mechanism by which these microbial products promote precipitation remains to be determined.

The inferred disulfide ligands in our precipitates probably would be reactive. They might participate in cross-linking, polymerization reactions that could explain how a monomer, like the hypothetical one in Figure 9, aggregates to make colloids. Similarly, the disulfide ligands, might form covalent bridges to the S_2^{2-} ions on pyrite surfaces or to organic polysulfides. Attachment of Mo to such materials has been proposed as scavenging mechanisms for Mo in nature.[10,68]

Jordisite—an example? Jordisite is a rare, dark gray-to-black sulfide that historically was believed to consist of x-ray amorphous MoS_2. Its composition is uncertain. Its structure is known to differ from that of both molybdenite and synthetic MoS_3, but is otherwise unknown.[69] Its particle sizes are invariably in the colloidal range. Miners recognize it by its ready conversion to molybdenum blue compounds when exposed to urine, a property inconsistent with molybdenite.[70] It forms in deep-seated groundwaters at temperatures up to 200°C and is often associated with uranium ores.[70-75] It is also found in hypogene zones of weathered molybdenum ore bodies.[76,77]

Owing to its colloidal nature, no pure jordisite is available for analysis. The few reported analyses include significant amounts of constituents other than Mo and S (for example: iron, silica and water). Previous workers have attributed the iron to contamination by colloidal iron sulfide particles. In Table 5, we recalculate the available published jordisite analyses so that the Fe is included in the empirical formulas. The resulting formulas seem too regular to be attributed to arbitrary mixtures of Fe and Mo sulfides. On the other hand, Fe/Mo mole ratios in jordisites cluster below 0.6, making them distinctly different from our aged precipitates. The solutions from which jordisite precipitates must differ significantly in composition and temperature from those in this

work. If jordisite colloids contain cuboid structures, then $FeMo_3S_4$ predominates over $Fe_2Mo_2S_4$. The findings here and in Ref.11 hint that nature may harbor a whole class of Fe-Mo-S colloids, of which jordisite is merely a member.

5. CONCLUSIONS

When mixtures of dissolved Fe and Mo are precipitated by sulfide, two colloidal products form. When Fe/Mo in solution exceeds unity, which is the usual case in nature, the early-formed colloidal products are composed of $FeMoS_4$ and poorly crystalline mackinawite. When dissolved Fe/Mo is less than unity, very little iron monosulfide persists, because it is nearly all converted to $FeMoS_4$. In either case, after only a few hours of aging, most $FeMoS_4$ spontaneously reduces irreversibly to a non-crystalline, Mo(IV) material. The reduced product is soluble in an oxidizing acid, concentrated HNO_3, but not in 1 M HCl. At the very lowest Fe/Mo investigated in this study, a further, very Fe-depleted colloidal phase forms.

Precipitates formed in these experiments appear to share a number of characteristics with Mo contained within sulfidic sediments (although information about the latter is still very limited). Both contain Mo in similar atomic environments, as indicated by similar Mo-S and Mo-Fe interatomic distances. Both appear to contain Mo(IV) rather than Mo(VI), and consequently both are dissolved only under oxidizing conditions. On the other hand, deposition of Mo via a $FeMoS_4$ precursor in the Black Sea requires $\{Fe^{2+}\}_{BS}$ or Q_{FeS} values that are several orders of magnitude greater than exist in bulk water and therefore requires positing existence of such values in microenvironments.

SUPPORTING INFORMATION

Section S1, description of turbidimetric and IPC analyses of peroxide digestion solutions; Figure S1, EXAFS spectra of run 7 with *k*-representation in the left panel and the Fourier transform shown in the right panel; Table S1, Black Sea data for Figure 8 and associated citations.

ACKNOWLEDGEMENTS

The authors thank Tais Dahl, Florian Sholz, two anonymous reviewers, and AE Sumit Chakraborty for constructive comments that significantly improved an earlier version of the manuscript. The authors express gratitude to Chad Wittkop for invaluable assistance with XRD analyses. TPV and AC thank the US National Science Foundation (Awards # EAR-1503567 and EAR-1503596) for funding this research. TPV and AC acknowledge the Donors of the American Chemical Society Petroleum Research Fund (PRF # 52201-UR2 and ACS-PRF 54583-DNI2) for supporting this research.

References

1) Lyons, T.W.; Reinhard, C.T.; Planavsky, N.J. *Nature.* The rise of oxygen in Earth's early ocean and atmosphere. **2014,** *506*, 307-315.
2) Smedley, P.L.; Kinniburgh, D.G. Molybdenum in natural waters: A review of the occurrence, distributions and controls. *Appl. Geochem.* **2017,** 84, 387-432.
3) Scott, C.; Lyons, T.W.; Bekker, A.; Shen, Y.; Poulton, S.W.; Chu, X.; Anbar, A.D. Tracing the stepwise oxygenation of the Proterozoic ocean. *Nature*. **2008,** *452*, 456-460.
4) Scott, C.; Lyons, T.W. Contrasting molybdenum cycling and isotopic properties in euxinic versus non-euxinic sediments and sedimentary rocks: Refining the paleoproxies. *Chem. Geol.* **2012,** *324-325*, 19-27.
5) Chappaz, A.; Lyons, T.W.; Gregory, D.D.; Reinhard, B.C.; Gill, C.; Large, R.R. Does pyrite act as an important host for molybdenum in modern and ancient euxinic sediments? *Geochim. Cosmochim. Acta.* **2014,** *74*, 203-214.
6) Wagner, M.; Chappaz, A.; Lyons, T.W. Molybdenum speciation and burial pathway in weakly sulfidic environments: Insights from XAFS. *Geochim. Cosmochim. Acta.* **2017,** *206*, 18-29.
7) Helz, G.R.; Miller, C.V.; Charnock, J.M.; Mosselmans, J.F.W.; Pattrick, R.A.D.; Garner, C.D.; Vaughan, D.J. Mechanism of molybdenum removal from the sea and its concentration in black shales: EXAFS evidence. *Geochim. Cosmochim. Acta.* **1996,** *60*, 3631-3642.
8) Helz, G.R.; Bura-Nakić, E.; Mikac, N.; Ciglenečki, I. New model for molybdenum behavior in euxinic waters. *Chem. Geol.* **2011,** *284*, 323-332.
9) Helz, G.R.; Erickson, B.E.; Vorlicek, T.P. Stabilities of thiomolybdate complexes of iron; implications for retention of essential trace elements (Fe, Cu, Mo) in sulfidic waters. *Metalomics.* **2014**, *6*, 1131-1140.
10) Freund, C.; Wishard, A.; Brenner, R.; Sobel, M.; Mizelle, J.; Kim, A.; Meyer, D.A.; Morford, J.A. The effect of a thiol-containing organic molecule on molybdenum adsorption onto pyrite. *Geochim. Cosmochim. Acta.* **2016**, *174*, 222-235.
11) Dahl, T.W.; Chappaz, A.; Hoek, J.; McKenzie, C.J.; Svane, S.; Canfield, D.E. Evidence of molybdenum association with particulate organic matter under sulfidic conditions. *Geobiol.* **2017,** *15*, 311-323.
12) Ardakani, O.H., Chappaz, A., Sanei, H. and Mayer, B. (2016) Effect of thermal maturity on remobilization of molybdenum in black shales. Earth Planet. Sci. Lett. 449, 311-320.
13) Korolev, D.F. The role of iron sulfides in the accumulation of molybdenum in sedimentary rocks of the reduced zone. *Geochemistry.* **1958,** *4*, 450-463.
14) Sugawara, K.; Okabe, S.; Tanaka, M. Geochemistry of molybdenum in natural waters (II). *J. Earth Sci. Nagoya Univ.* **1961**, *9*, 114-128.
15) Bertine, K.K. The deposition of molybdenum in anoxic waters. *Mar. Chem.* **1972,** *1*, 43-53.
16) Volkov, I.I.; Fomina, L.S. Influence of organic material and processes of sulfide formation on distribution of some trace elements in deep-water sediments of Black Sea. In: E.T. Degens and D.A. Ross (eds) The Black Sea: Geology, chemistry and Biology. Amer. Assoc. Petroleum Geol. Memoir 20, p. 456-476, 1974.
17) Huerta-Diaz, M.A.; Morse, J.W. Pyritization of trace metals in anoxic marine sediments. *Geochim. Cosmochim. Acta.* **1992,** *56*, 2681-2702.
18) Dahl, T.W.; Chappaz, A.; Fitts, J.P.; Lyons, T.W. Molybdenum reduction in a sulfidic lake: Evidence from x-ray absorption fine-structure spectroscopy and implications for the Mo paleoproxy. *Geochim. Cosmochim. Acta.* **2013,** *103*, 213-231.

19) Ardakani, O.H.; Chappaz, A.; Sanei, H.; Mayer B. Effect of thermal maturity on remobilization of molybdenum in black shales. *Earth Planet. Sci. Lett.* **2016,** 449, 311-320.
20) Havig, J.R.; McCormic,k M.L.; Hamilton, T.L.; Kump, L.R. The behavior of biologically important trace elements across the oxic/euxinic transition of meromictic Fayetteville Green Lake, New York, USA. *Geochim. Cosmochim. Acta.* **2015,** 165, 389-406.
21) Mohajerin, T.J.; Helz, G.R.; Johannesson, K.H. Tungsten-molybdenum fractionation in estuarine environments. *Geochim. Cosmochim. Acta.* **2016,** *177*, 105-119.
22) Buffle, J.; Zali, O.; Zumstein, J.; De Vitre, R. Analytical methods for the direct determination of inorganic and organic species: Seasonal changes of iron, sulfur, and pedogenic and aquagenic organic constituents in the eutrophic lake Bret, Switzerland. *Sci. Total Environ*. **1987**, *664*, 41-59.
23) Skei, J.M. Formation of framboidal iron sulfide in the water of a permanently anoxic fjord—Framvaren Fjord, south Norway. *Mar. Chem.* **1988.,** *3*, 345-352.
24) Lewis, B.L; Landing, W.M. The biogeochemistry of manganese and iron in the Black Sea. *Deep-Sea Res.* **1991**, *38*, S773-S803.
25) Muramoto, J.A.; Honjo, S.; Fry, B.; Hay, B.J.; Howarth, R.W.; Cisne, J.L. Sulfur, iron and organic carbon fluxes in the Black Sea: sulfur isotopic evidence for origin of sulfur fluxes. *Deep-Sea Res.* **1991,** *38 Suppl. 2*, S1151-S1187.
26) Perry, K.A.; Pedersen, T.F. Sulphur speciation and pyrite formation in meromictic ex-fjords. *Geochim. Cosmochim. Acta.* **1993**, *57*, 4405-4418.
27) Wilkin, R.T.; Barnes, H.L. Pyrite formation in an anoxic estuarine basin. *Amer. J. Sci. 297*, 620-650.
28) Cutter, G.A.; Kluckhohn, R.S. The cycling of particulate carbon, nitrogen, sulfur and sulfur species (iron monosulfide, greigite, pyrite and organic sulfur) in the water columns of Framvaren Fjord and the Black Sea. *Mar. Chem.* **1999**, *67*,149-160.
29) Li, X.; Cutter, G.A.; Thunell, R.C.; Tappa, E.; Gilhooly, W.P.III; Lyons, T.W.; Astor, Y.; Scranton, M.I. Particulate sulfur species in the water column of the Cariaco Basin. *Geochim. Cosmochim. Acta.* **2011**, *75*,148-163.
30) Bura-Nakić, E.; Viollier E.; Ciglenečki, I. Electrochemical and Colorimetric Measurements Show the Dominant Role of FeS in a Permanently Anoxic Lake. *Environ. Sci. Technol.* ***2013***, *47*, 741-749.
31) Lohmayer, R.; Reithmaier, G.M.S.; Bura-Nakić, E.; Planer-Friedrich, B. Ion-pair chromatography coupled to inductively coupled plasma-mass spectrometry (IPC-ICP-MS) as a method for thiomolybdate speciation in natural waters. *Anal. Chem.* **2015**, *87*, 3388-3395.
32) Vorlicek, T.P.; Chappaz, A.; Groskreutz, L.M.; Young, N.; Lyons, T.W. A new analytical approach to determining Mo and Re speciation in sulfidic waters. *Chem. Geol.* **2015**, *403*, 52-57.
33) Chandrasekaran, J., Ansari, M.A.; Sarkar, S. Aging of ammonium tetrathiomolybdate(VI) in air: An example of induced electron transfer by external oxidant, oxygen. *J. Less Common Met.* **1987**, 134, L23-L25.
34) Erickson, B.E.; Helz, G.R. Molybdenum(VI) speciation in sulfidic waters: Stability and lability of thiomolybdates. *Geochim. Cosmochim. Acta*. **2000**, *64*, 1149-1158.
35) Erickson, B.E. The speciation of molybdenum in sulfidic natural waters. Ph.D. dissertation. University of Maryland, College Park, 1998.

36) Vorlicek, T.P. Toward a better understanding of molybdenum fixation in sediments: The roles of mineral catalysis, zero-valent sulfur, and metal sulfides. Ph.D. dissertation. University of Maryland, College Park, 2002.
37) Ravel, Á.; Newville, M.. ATHENA, ARTEMIS, HEPHAESTUS: data analysis for X-ray absorption spectroscopy using IFEFFIT. *J. Synchrotron Radiat*, **2005**, *12*, 537–541.
38) Bura-Nakić, E.; Krznarić, D., Helz, G.R.; Ciglenečki, I. Characterization of iron sulfide species in model solutions by cyclic voltammetry. Revisiting an old problem. *Electroanal.* **2011**, *23*, 1376-1382.
39) Krznarić, D.; Ciglenečki, I. Voltammetric study of an FeS layer on a Hg electrode in supersaturated FeS chloride solution. *Environ. Chem.* 2015, *12*, 123-129.
40) Davison, W.; Phillips, N.; Tabner, B.J. Soluble iron sulfide species in natural waters: Reappraisal of their stoichiometry and stability constants. *Aquatic Sci.* **1999**, *61*, 23-43.
41) King, D. W.; Farlow, R. Role of carbonate speciation on the oxidation of Fe(II) by H_2O. *Mar. Chem.* **2000,** *70*, 201-209.
42) Rickard, D. Experimental concentration-time curves for the iron(II) sulphide precipitation process in aqueous solutions and their interpretation. *Chem. Geol.* **1989,** *78*, 315-324.
43) Bourdoiseau, J.-A.; Jeannin, M.; Sabot, R.; Rémazeilles C.; Refait, Ph. Characterisation of mackinawite by Raman spectroscopy: Effects of crystallization, drying and oxidation. *Corrosion Sci.* **2008**, *50*, 3247-3255.
44) Benning, L.G.; Wilkin, R. T.; Barnes, H.L. Reaction pathways in the Fe-S system below 100^{o}C. *Chem. Geol.* **2000**, *167*, 25-51.
45) Wolthers, M.; Charlet, L.; Der Linde, P.R.; Rickard, D.; van der Weijden, C.H. Surface chemistry of disordered mackinawite (FeS). *Geochim. Cosmochim. Acta.* **2005**, *69*, 3469-3481.
46) Wagman, D.D.; Evans, W.H.; Parker, V.B.; Schumm, R.H.; Halow, I.; Bailey, S.M.; Chruney, K.L.; Nuttall, R.L. The NBS tables of chemical thermodynamic properties. Selected values for inorganic and C_1 and C_2 organic substances in SI units. *J. Phys. Chem. Ref. Data*. **1982**, *11(Suppl. 2).*
47) Wolthers, M; van der Gaast, SJ; Rickard, D. The structure of disordered mackinawite. *Amer. Min.* **2003,** *88*, 2007-2015.
48) Jeong, HY; Lee, JH; Hayes, KF. Characterization of synthetic nanocrystalline mackinawite: Crystal structure, particle size, and specific surface area. *Geochim. Cosmochim. Acta.* **2008,** *72*, 493-505.
49) Lennie, A.R.; Redfern, S.A.T.; Schofield, P.F.; Vaughan, D.J. Synthesis and Rietveld crystal structure refinement of mackinawite, tetragonal FeS. *Min. Mag.* **1995**, *59*, 677-683.
50) Nissenbaum, A.; Swaine, D.J. Organic matter-metal interactions in recent sediments: The role of humic substances. *Geochim. Cosmochim. Acta* **1975**, 40, 809-816.
51) Quagraine, E.K.; Georgakaki, I.; Coucouvanis, D. Reactivity and kinetic studies of $(NH_4)_2(MoS_4)$ in acidic aqueous solution: Possible relevance to the angiostatic function of the MoS_4^{2-} ligand. *J. Inorg. Biochem.* **2009**, *103*, 143-155.
52) Weber, Th.; Muijsers, J.C.; Niemantsverdriet, J.W. (1995) Structure of amorphous MoS_3. *J. Phys. Chem.* **99**, 9194-9200.
53) Walton, R.I.; Dent, A.J.; Hibble, S.J. In situ investigation of the thermal decomposition of ammonium tetrathiomolybdate using combined time-resolved x-ray absorption spectroscopy and x-ray diffraction. *Chem. Mat.* **1998**, *10*, 3737-3745.
54) Hibble, SJ; Wood G.B. Modeling the structure of amorphous MoS_3: A neutron diffraction and reverse Monte Carlo Study. *J. Amer. Chem. Soc.* **2003**, *126*, 959-965.

55) Vorlicek, T.P.; Kahn, M.D.; Kasuya, Y.; Helz, G.R. Capture of molybdenum in pyrite-forming sediments: Role of ligand-induced reduction by polysulfides. *Geochim. Cosmochim. Acta.* **2004,** *68*, 547-556.

56) Davison, W.) The solubility of iron sulphides in synthetic and natural waters at ambient temperature. *Aquatic Sci.* **1991,** *53*, 309-329.

57) Kowalski, N; Dellwig O.; Beck M.; Gräwe U.; Neubert N.; Nägler T.F.; Badewien T.H.; Brumsack H.-J.; van Beusekom J.E.E.; Böttcher M.E. Pelagic molybdenum concentration anomalies and the impact of sediment resuspension on the molybdenum budget in two tidal systems of the North Sea. Geochim. Cosmochim. Acta **2013**, *119*, 198-211.

58) Morford, J.L; Emerson, S.R.; Breckel, E.J.; Kim, S.H. Diagenesis of oxyanions (V, U, Re, and Mo) in pore waters and sediments from a continental margin. *Geochim. Cosmochim. Acta*, **2005,** *69*, 5021-5032.

59) McManus, J.; Berelson, W.M.; Severmann, S.; Poulson, R.L.; Hammond, D.E.; Klinkhammer, G.P.; Holm C. Molybdenum and uranium geochemistry in continental margin sediments: Paleoproxy potential. *Geochim. Cosmochim. Acta*, **2006**, *70*, 4643-4662.

60) Raiswell, R.; Canfield, D.E. Sources of iron for pyrite formation in marine sediments. *Amer. J. Sci.* **1998**, *298*, 219-245.

61) Xu, J.; Qian, J.; Wei, Q. Synthesis and structure of a novel molybdenum-iron-sufur cluster with Mo_2Fe_2 core and all-disulfide chelate ligands, $\{Mo_2Fe_2(\mu_3\text{-}S)_4(S_2CNEt_2)_5\}CH_3CN$. *Inorg. Chim. Acta.* **1989**, *164*, 55-58.

62) Kawaguchi, H.; Yamada, K.; Ohnishi, S.; Tatsumi, K. Construction of a cyclic tricubane cluster $\{Cp^*_2Mo_2Fe_2S_4\}(\mu\text{-}S_4)_3$ from the $Mo_2Fe_2S_4$ single cubane component. *J. Amer. Chem. Soc.* **1997**, *119*, 10871-10872.

63) Koutmos, M.; Georgakaki, I.P.; Tsiolis, P.; Coucouvanis, D. Synthesis and characterization of $MoFe_3S_4$ and $Mo_2Fe_2S_4$ single cubanes. *Z. Anorg. Allg. Chem.* **2008**, *634*, 255-261.

64) Melnik, M.; Ondrejkovicova, I.; Sundberg, M. R.; Holloway, C.E. Crystallographic and structural analysis of iron heterometallic compounds. Part III. Heterotetranuclear compounds. *Rev. Inorg. Chem.* **2008**, *28*, 237-456.

65) Shibahara, T.; Sakane, G.; Naruse, Y.; Taya, K.; Akashi, H., Ichimura, A.; Adachi, H. Syntheses and characterization of cubane-type clusters with molybdenum-iron-sulfur (Mo_3FeS_4) or molybdenum-nickel-sulfur (Mo_3NiS_4) cores. X-ray structures of $\{Mo_3FeS_4(H_2O)_{10}\}(CH_3C_6H_4SO_3)_4{\cdot}7H_2O$ and $\{Mo_3FeS_4(H_2O)(NH_3)_9\}Cl_4$, and discrete variational (DV)-Xα calculation of the electronic structures of $\{Mo_3FeS_4(H_2O)_{10}\}^{4+}$, $\{Mo_3FeS_4(H_2O)(NH_3)_9\}^{4+}$ and $\{Mo_3NiS_4(H_2O)_{10}\}^{4+}$. *Bull. Chem. Soc. Japan.* **1995**, *68*, 2769-2782.

66) Müller, A.; Hildebrand, A.; Penk, M.; Bögge, H. $\{Fe_2S_2(MoS_4)_2\}^{4-}$: The first complex with two MoS_4^{2-} ions coordinated to a ferredoxin type central unit. *Inorg. Chim. Acta.* **1988,** *148*,11-13.

67) Teo, B.-K.; Antonio, M.R.; Averill, B.A. Molybdenum K-edge extended x-ray absorption fine structure (EXAFS) studies of synthetic Mo-Fe-S clusters containing the MoS_4 unit: Development of a fine adjustment technique based on models. *J. Amer. Chem. Soc.* **1983**, *105*, 3751-3762.

68) Bostick, B.C.; Fendorf, S.; Helz, G.R. Differential adsorption of molybdate and tetrathiomolybdate on pyrite (FeS_2). *Environ. Sci. Technol.* **2003**, *37*, 285-291.

69) Diemann, E. Zur Struktur des natürlichen amorphen Molybdänsulfids (Jordisite) *Naturwissen.* **1976**, *63*, 385-386.

70) Cunningham, C.G.; Rasmussen, J.D.; Steven, T.A.; Rye, R.O.; Rowley, P.D.; Romberger, S.B.; Selverstone, J. Hydrothermal uranium deposits containing molybdenum and fluorite in the Marysvale volcanic field, west-central Utah. *Mineralium Deposita* **1998**, *33*, 477-494.
71) Granger, H.C.; Ingram, B.L. Occurrence and indentification of jordisite at Ambrosia Lake, New Mexico. *U.S. Geol. Survey Prof. Paper*. **1966**, *550-B*, B120-B124.
72) Cheney, E.S.; Trammell, J.W. Isotopic evidence for inorganic precipitation of uranium roll ore bodies. *Amer. Assoc. Petrol. Geol. Bull.* **1973**, *57*, 1297-1304.
73) Brookins, D.G. Position of uraninite and/or coffinite accumulations to the hematite/pyrite interface in sandstone-type deposits. *Econ. Geol.* **1976**, *71*, 944-948.
74) Hofmann, B.A.; Helfer, M.; Diamond, L.W.; Villa, I.M.; Frei, R.; Eikenberg, J. Topography-driven hydrothermal breccia mineralization of Pliocene age at Grimsel Pass, Aar massif, Central Swiss Alps. *Schweiz. Mineral. Petrograph. Mitteilungen.* **2004**, *84*, 271-302.
75) Saunders, J.A.; Pivetz, B.E.; Voorhies, N.; Wilkin, R.T. Potential aquifer vulnerability in regions down-gradient from uranium in situ recovery (ISR) sites. *J. Environ. Monit.* **2016**, *183*, 67-83.
76) Clark, A.H. Molybdenite $2H_1$, molybdenite 3R, and jordisite from Carrizal Alto, Atacama, Chile. *Amer. Min.* **1971,** *56*, 1832-1835.
77) LeAnderson, J.P.; Schrader, E.L.; Brake, S.; Kaback, D.S. Behavior of molybdenum during weathering of the Ceresco Ridge porphyry molybdenite deposit, Climax, Colorado and a comparison with the Hollister deposit, North Carolina. *Appl. Geochem.* **1987,** *2*, 399-416.
78) Staples, L.W. Ilsemannite and jordistie. *Amer. Min.* **1951,** *36*, 609-614.
79) Kao, L-S.; Peacor, D.R.; Coveney, R. M. Jr.; Zhao, G.; Dungey K.E.; Curtis M.D.; Penner-Hahn J.E. A C/MoS_2 mixed-layer phase (MoSC) occurring in metalliferous black shales from southern China, and new data on jordisite. *Amer. Min.* **2001**, *86*, 852-861.
80) Orberger, B.; Vymazalova, A.; Wagner, C.; Fialin, M.; Gallien, J.P.; Wirth, R.; Pasava, J.; Montagnac, G. Biogenic origin of intergrown Mo-sulphide- and carbonaceous matter in Lower Cambrian black shales (Zunyi Formation, southern China). *Chem. Geol.* **2007,** *238*, 213-231.

Table 1. Experimental data. All runs contained 20 mM borate buffer. After about 100 h of reaction, 0.1 M $MgCl_2$ was added to promote flocculation.

Run	Initial ΣMo (M)	Initial ΣFe (M)	React. time (h)	Final ΣMo (M)	Final ΣFe (M)	Final pH	Final ΣS^{-II} (M)	Final MoS_4^{2-} (M)	$N_{Fe/Mo}$‡ Initial
1	6.62E-04	6.62E-05	404	5.20E-04	5.28E-05	8.35	8.76E-03	5.11E-04	0.100
2	4.63E-04	6.62E-05	385	4.28E-04	5.00E-05	8.33	9.22E-03	3.67E-04	0.143
3	3.31E-04	6.62E-05	2328	2.68E-04	4.96E-05	8.37	7.41E-03	2.27E-04	0.200
4	6.78E-05	1.36E-05	355	6.50E-05	5.24E-06	8.22	7.65E-03	5.14E-05	0.201
5	6.81E-05	2.27E-05	811	6.43E-05	1.30E-05	8.07	4.66E-03	4.68E-05	0.333
6	1.99E-04	6.62E-05	2592	1.61E-04	5.39E-05	8.23	3.07E-03	1.04E-04	0.333
7	1.32E-04	6.62E-05	2760	9.16E-05	3.02E-05	8.23	6.67E-03	5.80E-05	0.502
8	6.81E-05	3.40E-05	980	6.31E-05	1.49E-05	8.23	6.91E-03	4.32E-05	0.499
9	6.62E-05	6.62E-05	3816	5.67E-05	3.10E-05	8.38	4.61E-03	1.93E-05	1.000
10	3.31E-05	6.62E-05	3168	2.00E-05	8.88E-06	8.18	5.44E-03	1.11E-05	2.000
11	6.81E-05	1.36E-04	1149	2.77E-05	1.35E-05	8.25	6.69E-03	1.17E-05	1.997
12	2.18E-05	6.62E-05	1656	1.96E-05	1.54E-05	8.31	3.61E-03	8.38E-06	3.037
13	6.78E-05	2.03E-04	979	5.85E-05	4.57E-05	8.03	7.21E-03	1.26E-05	2.994
14	6.78E-05	3.39E-04	810	4.86E-05	3.30E-05	8.07	8.72E-03	8.97E-06	5.000
15	6.78E-05	4.75E-04	356	3.09E-05	2.91E-05	8.08	6.56E-03	4.42E-06	7.006
16	6.78E-05	6.76E-04	356	4.05E-06	8.90E-07	8.03	5.96E-03	5.00E-07	9.971
17	0	6.62E-05	1610	0	2.45E-06	8.33	6.77E-03	0	∞
18*	6.78E-05	6.76E-04	314	2.39E-05	2.91E-05	8.01	5.86E-03	4.90E-06	9.971

‡ $N_{Fe/Mo}$ is the initial mole ratio of total Fe to total Mo.
* Sulfur saturated.

Table 2. Results from thermodynamic speciation calculations.

Run	HS^- (M)	Fe^{2+} (M)	$Fe(HS)_2^0$ (M)	$[(FeS)_2(MoS_4)_2]^{4-}$ (M)	ΣMo calc (M)	log Q_{FeS}	log Q_{MoS3}
1	6.47E-03	2.47E-11	3.84E-10	2.52E-05	5.98E-04	1.80	-16.87
2	7.22E-03	3.16E-11	6.09E-10	2.40E-05	4.38E-04	1.93	-17.04
3	6.12E-03	5.42E-11	7.52E-10	2.35E-05	2.93E-04	2.14	-17.22
4	7.08E-03	9.40E-11	1.75E-09	2.43E-06	5.90E-05	2.29	-17.78
5	4.14E-03	4.19E-10	2.67E-09	6.24E-06	6.00E-05	2.55	-17.46
6	2.27E-03	4.54E-10	8.68E-10	2.50E-05	1.73E-04	2.49	-16.99
7	6.07E-03	2.32E-10	3.18E-09	1.45E-05	9.13E-05	2.62	-17.67
8	6.38E-03	2.07E-10	3.12E-09	7.07E-06	6.03E-05	2.59	-17.82
9	4.23E-03	6.95E-10	4.60E-09	1.39E-05	5.25E-05	3.09	-18.14
10	5.12E-03	8.66E-10	8.40E-09	4.15E-06	2.06E-05	2.87	-17.92
11	6.32E-03	6.99E-10	1.03E-08	6.35E-06	2.58E-05	3.13	-18.4
12	3.41E-03	1.62E-09	6.96E-09	6.70E-06	2.47E-05	3.30	-18.34
13	6.52E-03	1.98E-09	3.11E-08	2.26E-05	5.86E-05	3.38	-18.17
14	8.02E-03	1.74E-09	4.14E-08	1.62E-05	4.21E-05	3.45	-18.44
15	6.06E-03	4.27E-09	5.81E-08	1.42E-05	3.36E-05	3.73	-18.64
16	5.58E-03	2.55E-09	2.95E-08	3.89E-07	2.40E-06	3.43	-19.03
17	6.56E-03	1.44E-07	2.29E-06	-	-	5.55	
18	4.58E-03	6.00E-09	4.66E-08	1.43E-05	3.42E-05	3.69	-18.4

Table 3: Mo average oxidation state for the precipitates derived from the relationship between E_m and the Mo oxidation state. See Fig.7.

Samples	E_m (eV)	Average Mo oxidation state
Reference materials		
$Mo(IV)S_2$	2.0030.0	4.0
$Mo(VI)S_4^{2-}$	20043.0	6.0
Runs		
6	20030.7	4.1
7	20030.1	4.0
9	20030.2	4.0
12	20030.5	4.1

Table 4. Molybdenum EXAFS data for selected precipitates.

Runs	Mo--S_1			Mo--S_2			Mo--Fe			Amp	R factor
	n	r (Å)	σ^2	n	r (Å)	σ^2	n	r (Å)	σ^2		
6	2	2.32±0.02	0.003	3	2.44±0.03	0.003	1	2.79±0.03	0.003	0.85	0.02
7	2	2.32±0.05	0.003	3	2.47±0.05	0.003	1	2.81±0.04	0.003	0.93	0.02
9	2	2.30±0.03	0.003	3	2.45±0.04	0.003	1	2.80±0.02	0.003	0.97	0.03
12	2	2.31±0.03	0.003	3	2.46±0.03	0.003	1	2.81±0.05	0.003	0.88	0.02

All σ_2 values were set to 0.003

Table 5. Atomic proportions of Fe, Mo and S in some jordisites and Fe-Mo-S precipitates.

Sample Type	Empirical Formula	Reference
Jordisites	$Fe_{0.61}MoS_{3.21}$	78
	$Fe_{0.28}MoS_{2.24}$	71
	$Fe_{0.39}MoS_{2.56}$	71
	$Fe_{0.48}MoS_{2.86}$	71
	$Fe_{0.40}MoS_{2.70}$	71
	$Fe_{0.31}MoS_{2.27}$	74
Cambrian ore mineral*	$(Fe,Ni)_{0.33}MoS_{2.67}C_{10}$*	79
Precipitates	$Fe_{0.78}MoS_{3.83}$	This work
	$Fe_{0.83}MoS_{3.75}$	This work
	$Fe_{0.63}MoS_{3.60}$	This work

*An exotic graphite intercolation compound that occurs as an ore mineral in metalliferous black shales in China.[79,80]

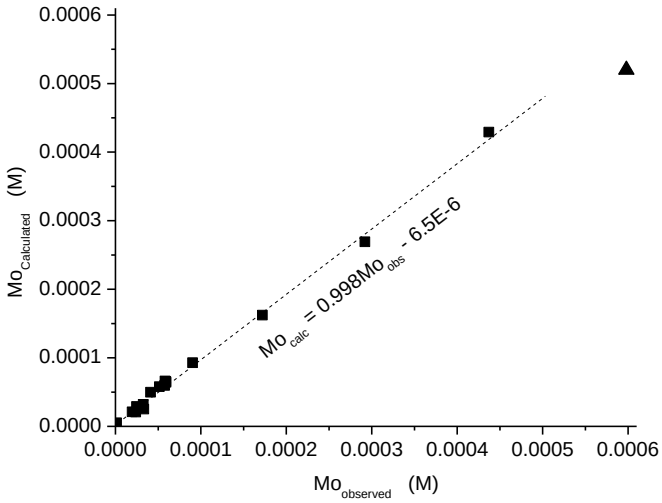

Figure 1. Excellent agreement of calculated total dissolved Mo with measured total dissolved Mo. Mo_{calc} is determined by summing the calculated concentrations of the dissolved Mo species (i.e. MoS_4^{2-} + $MoOS_3^{2-}$ + $[FeO(OH)MoS_4]^{3-}$ + $2[(FeS)_2(MoS_4)_2]^{4-}$). The point represented by a triangle at the highest dissolved Mo concentration deviates from the trend of the remaining data and was excluded from the regression.

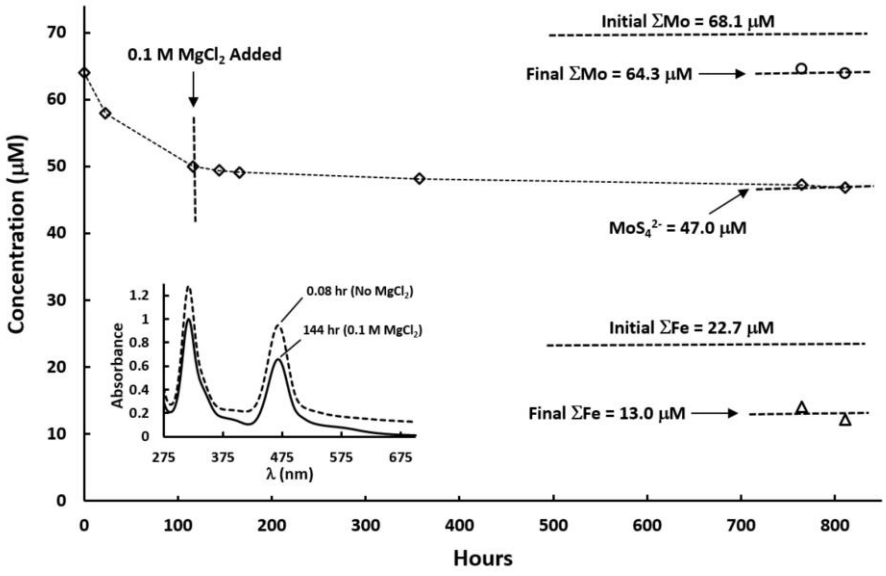

Figure 2. Typical time course for a run (here, Run 5; see Table 1).

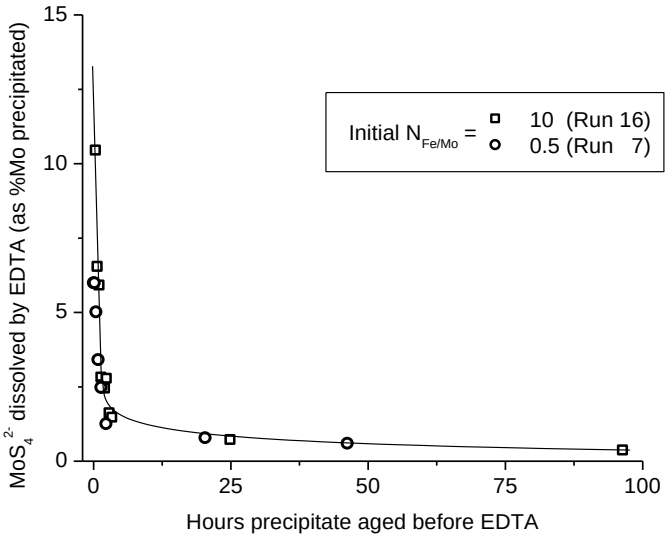

Figure 3. Reversal of the precipitation process by 0.001 M EDTA after various aging times. Beyond the first day, most of the precipitated MoS_4^{2-} is no longer released by this treatment.

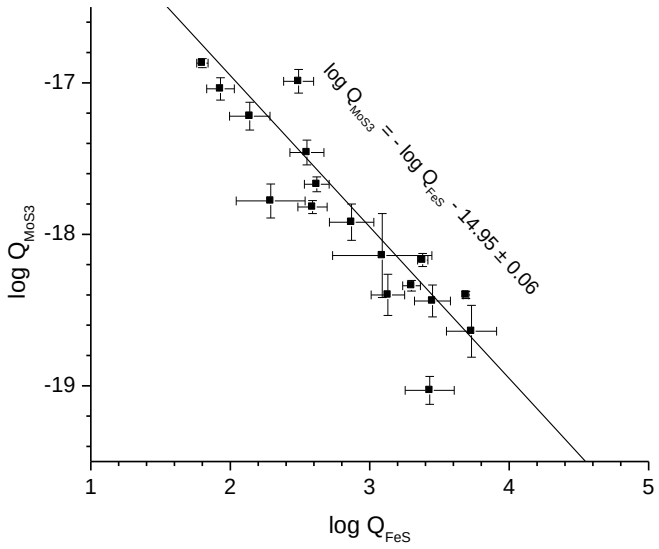

Figure 4. Gibbs-Duhem plot relating the chemical potentials of MoS_3 and FeS components (data in Table 2). Error bars display analytical uncertainties that have been propagated through the thermodynamic speciation calculations by the root-mean-square method. The line is an error-weighted regression line with slope forced to -1.0 (R^2 0.95). The ±0.06 uncertainty in the intercept is the standard error.

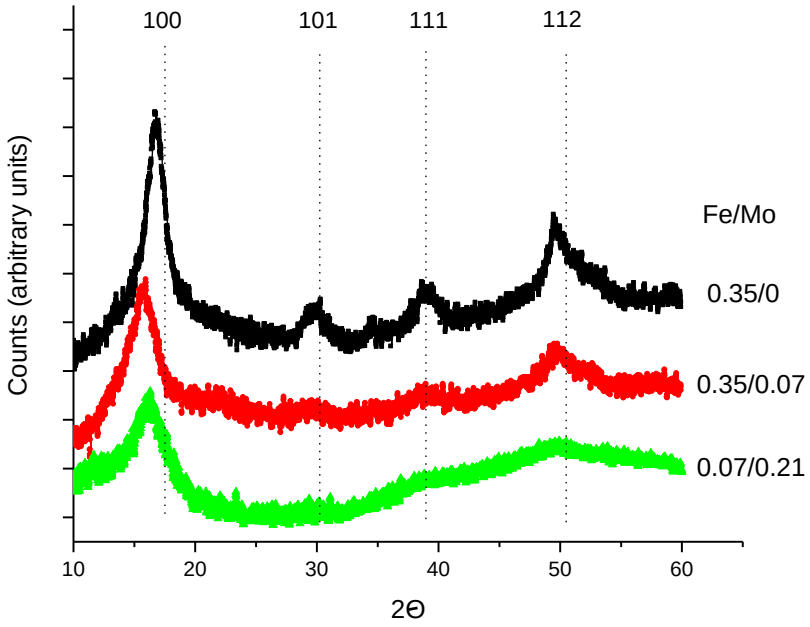

Figure 5. X-ray diffraction patterns (Cu Kα radiation) for three freeze-dried products (polynomial background correction). Labels at the right side of the figure give initial concentrations (mM) of Fe^{2+} and MoS_4^{2-} in the solutions that produced the precipitates. Dotted vertical lines show positions of major peaks for crystalline mackinawite.[49]

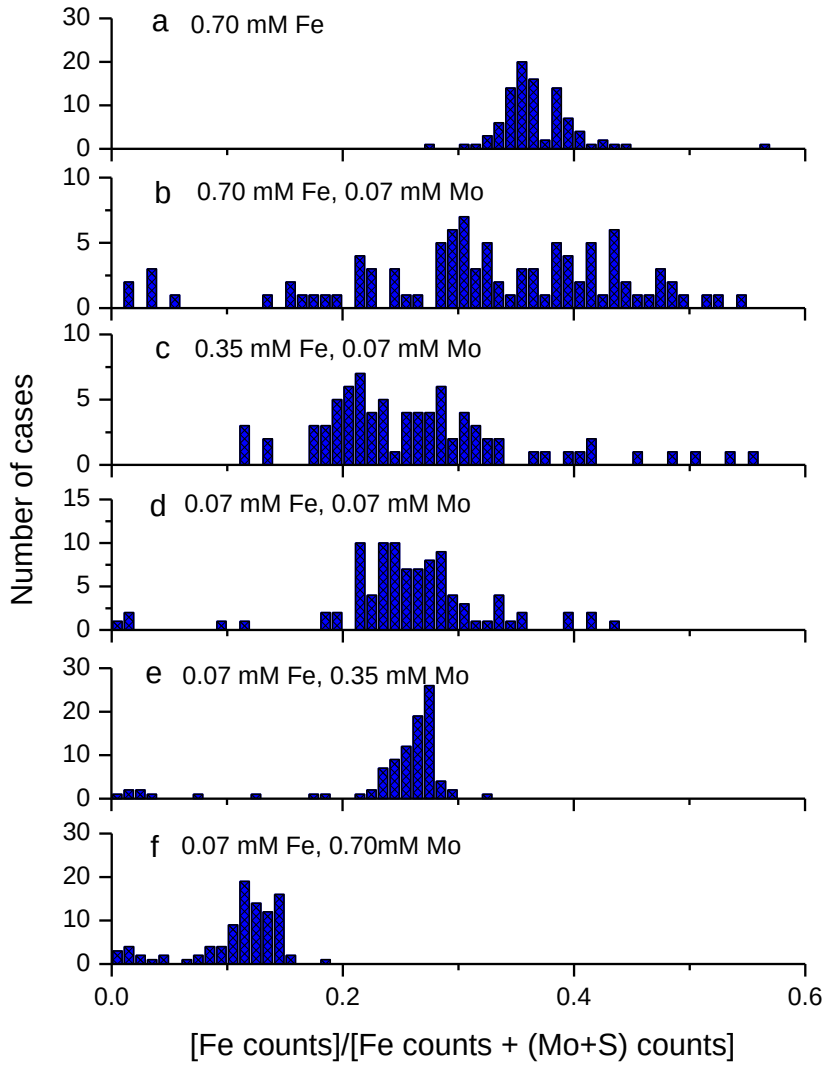

Figure 6. Histograms showing the ratio of EDS counts for Fe to the sum of counts for Fe plus overlapping counts for Mo + S in test precipitates. Counts for Mo and S have nearly the same energy and could not be measured independently. Test precipitates were taken from mother solutions initially containing 10 mM ΣS^{2-} and 20 mM borate buffer at pH 8.5 as well as (panel a) 0.70 mM Fe^{2+}, (panel b) 0.70 mM Fe^{2+} and 0.07 mM $MoS4^{2-}$, (panel c) 0.35 mM Fe^{2+} and 0.07 mM $MoS4^{2-}$, (panel d) 0.07 mM Fe^{2+} and 0.07 mM $MoS4^{2-}$, (panel e) 0.07 mM Fe^{2+} and 0.35 mM $MoS4^{2-}$, and (panel f) 0.07 mM Fe^{2+} and 0.70 mM $MoS4^{2-}$.

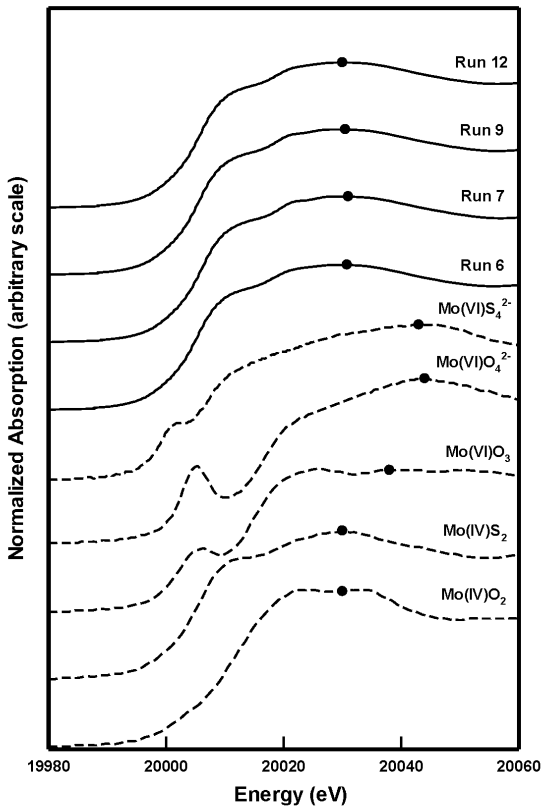

Figure 6

Figure 7: XANES spectra of samples (solid lines) and Mo reference compounds (dashed lines). The black dots identify the maximum absorption energy (E_m).

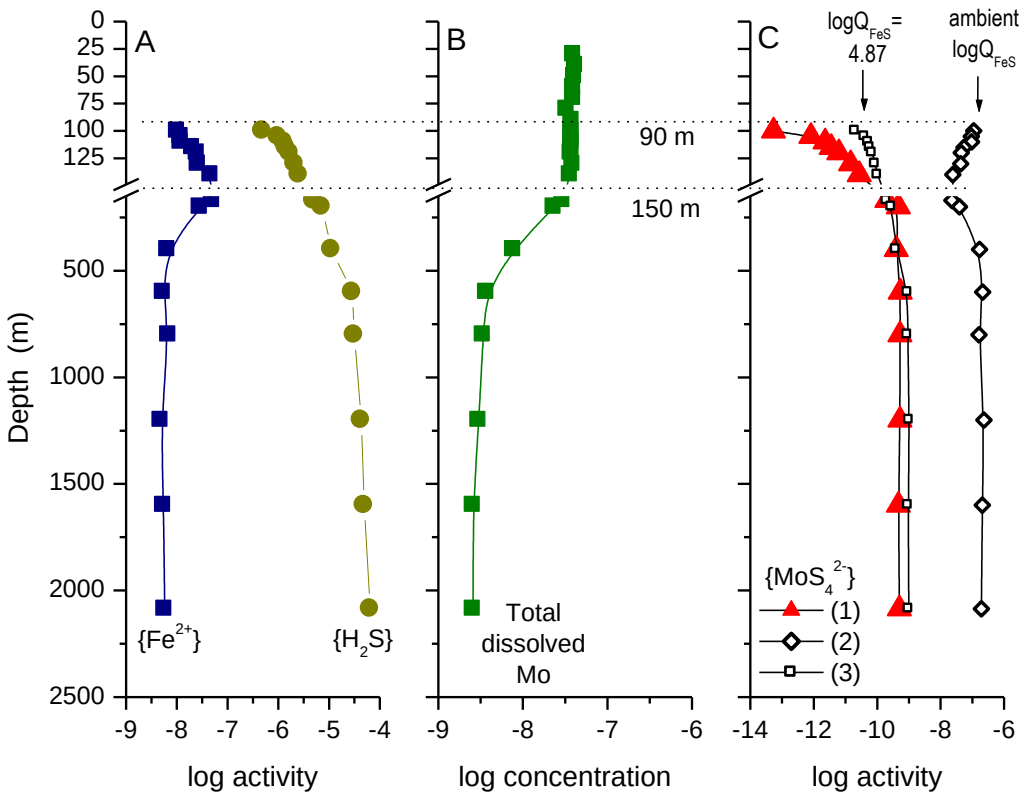

Figure 8. Black Sea data. Panel A: Profiles of thermodynamic activities of Fe^{2+} and H_2S in the sulfidic waters of the Black Sea calculated from water analyses. Panel B: Observed concentration of dissolved Mo from water analyses. Panel C: Curve 1, $\{MoS_4^{2-}\}_{BS}$ calculated from water analyses. Curve 2, $\{MoS_4^{2-}\}_{eq}$ at equilibrium with $FeMoS_4$ if log Q_{FeS} at each depth is calculated from water analyses. Curve 3, $\{MoS_4^{2-}\}_{eq}$ if log Q_{FeS} is fixed at 4.9. Activities and concentrations on molar scale. See Table S1 for sources of data.

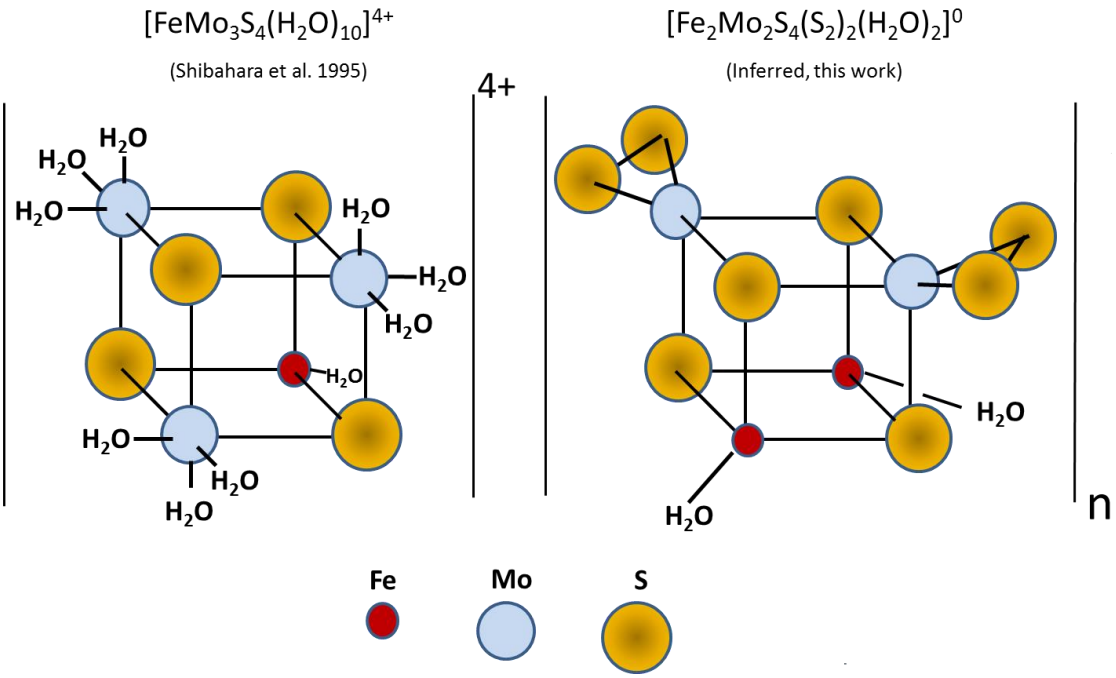

Figure 9. *Left:* Structure of an idealized aqueous cuboidal cluster cation, $[FeMo_3S_4(H_2O)_{10}]^{4+}$;[65] actual heterometallic cuboid structures are distorted from perfect cubic symmetry. *Right:* hypothetical monomer produced in this work. Mo-S interatomic distances in the $[FeMo_3S_4(H_2O)_{10}]^{4+}$ cation range from 2.344 to 2.356 Å compared to averages of 2.31 and 2.46 Å in our precipitates; Mo-Fe distances in $[FeMo_3S_4(H_2O)_{10}]^{4+}$ are 2.660 to 2.681 Å but average 2.80 Å in our precipitates. The cation has Mo-Mo distances of 2.77 Å, but a Mo-Mo shell was not resolved in our amorphous precipitates, possibly due to disorder.

Table of Contents Art

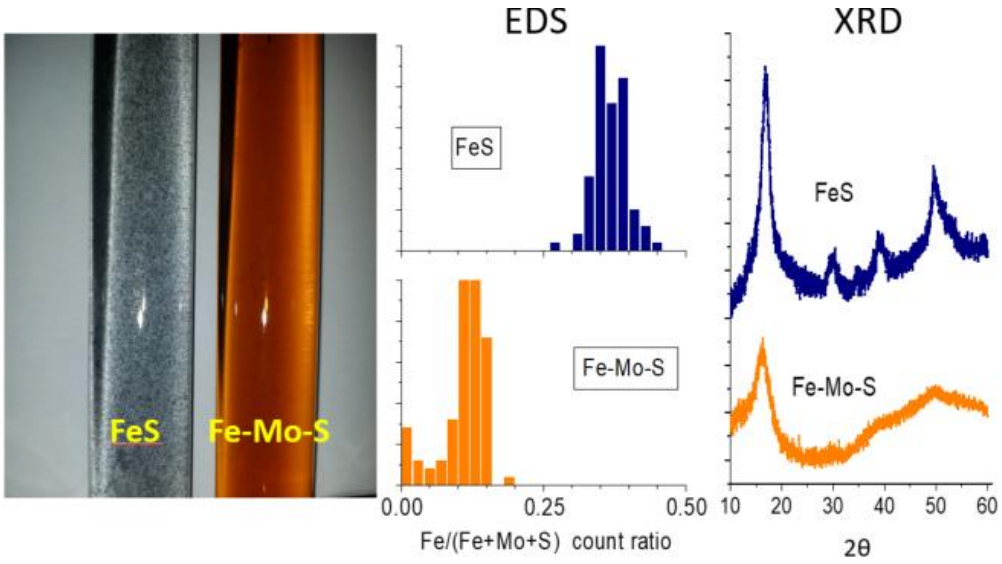

Run	Initial ΣMo (M)	Initial ΣFe (M)	React. time (h)	Final ΣMo (M)	Final ΣFe (M)	Final pH	Final ΣS^{-II} (M)	Final MoS_4^{2-} (M)	$N_{Fe/Mo}$ ‡ Initial
1	6.62E-04	6.62E-05	404	5.20E-04	5.28E-05	8.35	8.76E-03	5.11E-04	0.100
2	4.63E-04	6.62E-05	385	4.28E-04	5.00E-05	8.33	9.22E-03	3.67E-04	0.143
3	3.31E-04	6.62E-05	2328	2.68E-04	4.96E-05	8.37	7.41E-03	2.27E-04	0.200
4	6.78E-05	1.36E-05	355	6.50E-05	5.24E-06	8.22	7.65E-03	5.14E-05	0.201
5	6.81E-05	2.27E-05	811	6.43E-05	1.30E-05	8.07	4.66E-03	4.68E-05	0.333
6	1.99E-04	6.62E-05	2592	1.61E-04	5.39E-05	8.23	3.07E-03	1.04E-04	0.333
7	1.32E-04	6.62E-05	2760	9.16E-05	3.02E-05	8.23	6.67E-03	5.80E-05	0.502
8	6.81E-05	3.40E-05	980	6.31E-05	1.49E-05	8.23	6.91E-03	4.32E-05	0.499
9	6.62E-05	6.62E-05	3816	5.67E-05	3.10E-05	8.38	4.61E-03	1.93E-05	1.000
10	3.31E-05	6.62E-05	3168	2.00E-05	8.88E-06	8.18	5.44E-03	1.11E-05	2.000
11	6.81E-05	1.36E-04	1149	2.77E-05	1.35E-05	8.25	6.69E-03	1.17E-05	1.997
12	2.18E-05	6.62E-05	1656	1.96E-05	1.54E-05	8.31	3.61E-03	8.38E-06	3.037
13	6.78E-05	2.03E-04	979	5.85E-05	4.57E-05	8.03	7.21E-03	1.26E-05	2.994
14	6.78E-05	3.39E-04	810	4.86E-05	3.30E-05	8.07	8.72E-03	8.97E-06	5.000
15	6.78E-05	4.75E-04	356	3.09E-05	2.91E-05	8.08	6.56E-03	4.42E-06	7.006
16	6.78E-05	6.76E-04	356	4.05E-06	8.90E-07	8.03	5.96E-03	5.00E-07	9.971
17	0	6.62E-05	1610	0	2.45E-06	8.33	6.77E-03	0	∞
18*	6.78E-05	6.76E-04	314	2.39E-05	2.91E-05	8.01	5.86E-03	4.90E-06	9.971

Table 1

Run	HS^- (M)	Fe^{2+} (M)	$Fe(HS)_2^0$ (M)	$[(FeS)_2(MoS_4)_2]^{4-}$ (M)	ΣMo calc (M)	log Q_{FeS}	log Q_{MoS3}
1	6.47E-03	2.47E-11	3.84E-10	2.52E-05	5.98E-04	1.80	-16.87
2	7.22E-03	3.16E-11	6.09E-10	2.40E-05	4.38E-04	1.93	-17.04
3	6.12E-03	5.42E-11	7.52E-10	2.35E-05	2.93E-04	2.14	-17.22
4	7.08E-03	9.40E-11	1.75E-09	2.43E-06	5.90E-05	2.29	-17.78
5	4.14E-03	4.19E-10	2.67E-09	6.24E-06	6.00E-05	2.55	-17.46
6	2.27E-03	4.54E-10	8.68E-10	2.50E-05	1.73E-04	2.49	-16.99
7	6.07E-03	2.32E-10	3.18E-09	1.45E-05	9.13E-05	2.62	-17.67
8	6.38E-03	2.07E-10	3.12E-09	7.07E-06	6.03E-05	2.59	-17.82
9	4.23E-03	6.95E-10	4.60E-09	1.39E-05	5.25E-05	3.09	-18.14
10	5.12E-03	8.66E-10	8.40E-09	4.15E-06	2.06E-05	2.87	-17.92
11	6.32E-03	6.99E-10	1.03E-08	6.35E-06	2.58E-05	3.13	-18.4
12	3.41E-03	1.62E-09	6.96E-09	6.70E-06	2.47E-05	3.30	-18.34
13	6.52E-03	1.98E-09	3.11E-08	2.26E-05	5.86E-05	3.38	-18.17
14	8.02E-03	1.74E-09	4.14E-08	1.62E-05	4.21E-05	3.45	-18.44
15	6.06E-03	4.27E-09	5.81E-08	1.42E-05	3.36E-05	3.73	-18.64
16	5.58E-03	2.55E-09	2.95E-08	3.89E-07	2.40E-06	3.43	-19.03
17	6.56E-03	1.44E-07	2.29E-06	0.00E+00	-	5.55	-
18	4.58E-03	6.00E-09	4.66E-08	1.43E-05	3.42E-05	3.69	-18.4

Table 2

Samples	E_m (eV)	Average Mo oxidation state
Reference materials		
$Mo(IV)S_2$	20030.0	4.0
$Mo(VI)S_4^{2-}$	20043.0	6.0
Runs		
6	20030.7	4.1
7	20030.1	4.0
9	20030.2	4.0
12	20030.5	4.1

Table 3

Runs	Mo--S_1			Mo--S_2			Mo--Fe			Amp	R factor
	n	r (Å)	σ^2	n	r (Å)	σ^2	n	r (Å)	σ^2		
6	2	2.32±0.02	0.003	3	2.44±0.03	0.003	1	2.79±0.03	0.003	0.85	0.02
7	2	2.32±0.05	0.003	3	2.47±0.05	0.003	1	2.81±0.04	0.003	0.93	0.02
9	2	2.30±0.03	0.003	3	2.45±0.04	0.003	1	2.80±0.02	0.003	0.97	0.03
12	2	2.31±0.03	0.003	3	2.46±0.03	0.003	1	2.81±0.05	0.003	0.88	0.02

All σ_2 value were set to 0.003

Table 4

Sample Type	Empirical Formula	Reference
Jordisites	$Fe_{0.61}MoS_{3.21}$	73
	$Fe_{0.28}MoS_{2.24}$	66
	$Fe_{0.39}MoS_{2.56}$	66
	$Fe_{0.48}MoS_{2.86}$	66
	$Fe_{0.40}MoS_{2.70}$	66
	$Fe_{0.31}MoS_{2.27}$	69
Cambrian ore mineral*	$(Fe,Ni)_{0.33}MoS_{2.67}C_{10}$*	74
Precipitates	$Fe_{0.78}MoS_{3.83}$	This work
	$Fe_{0.83}MoS_{3.75}$	This work
	$Fe_{0.63}MoS_{3.60}$	This work

*An exotic graphite intercolation compound that occurs as an ore mineral in metalliferous black shales in China.[74,75]

Table 5

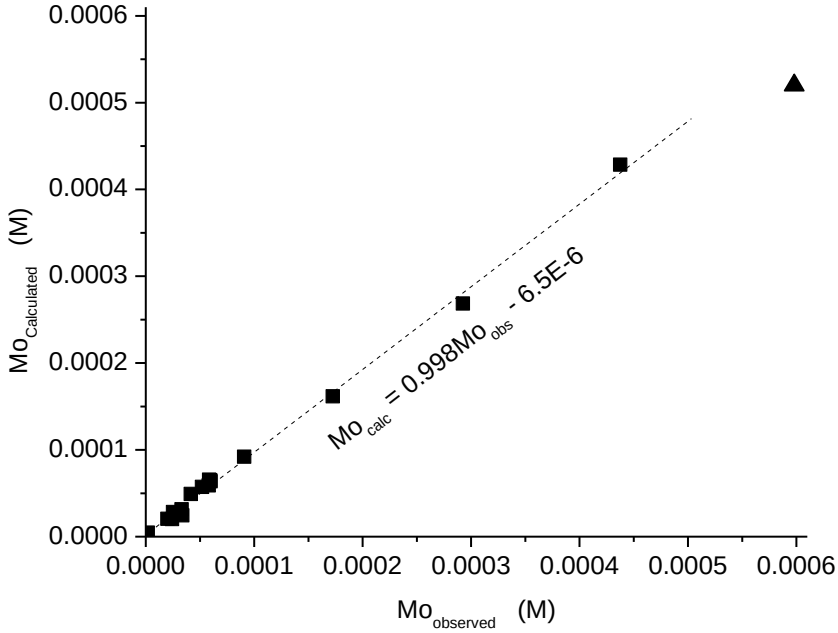
0.0006
0.0005
0.0004
0.0003
0.0002
0.0001
0.0000
Mo Calculated (M)
0.0000
0.0001
0.0002
0.0003
0.0004
0.0005
0.0006
Mo observed (M)
Mo calc = 0.998Mo obs - 6.5E-6

Figure 1

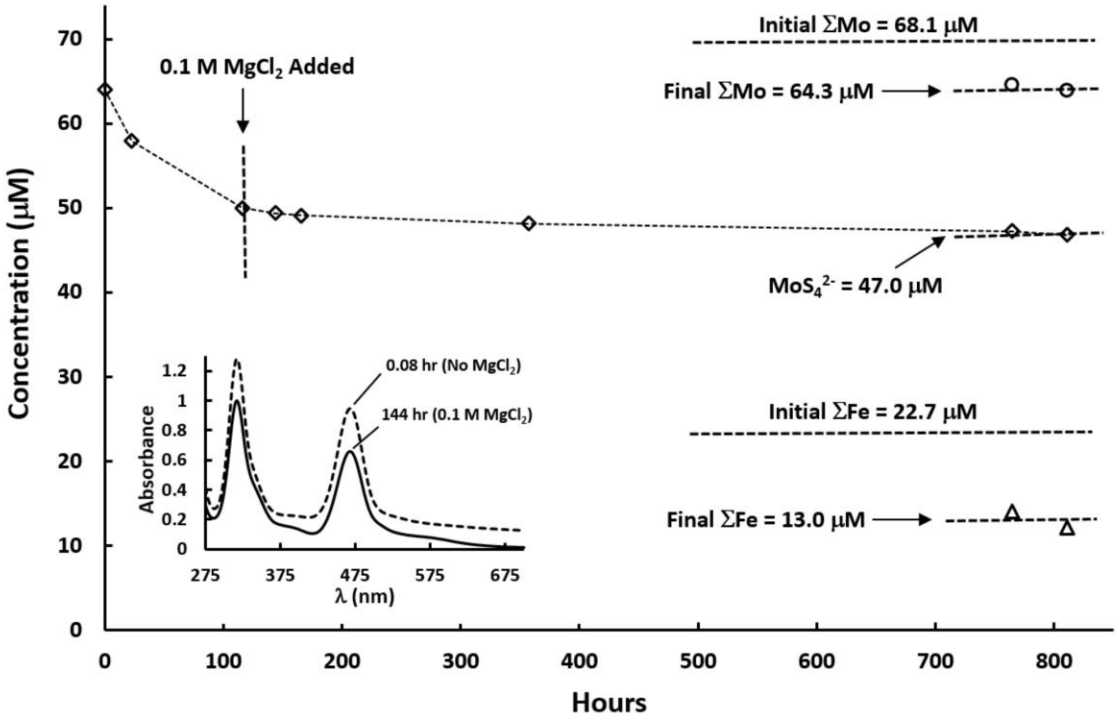
Initial ΣMo = 68.1 μM
0.1 M MgCl2 Added
Final ΣMo = 64.3 μM
MoS4 2- = 47.0 μM
Concentration (μM)
Hours
0.08 hr (No MgCl2)
144 hr (0.1 M MgCl2)
Absorbance
λ (nm)
Initial ΣFe = 22.7 μM
Final ΣFe = 13.0 μM

Figure 2

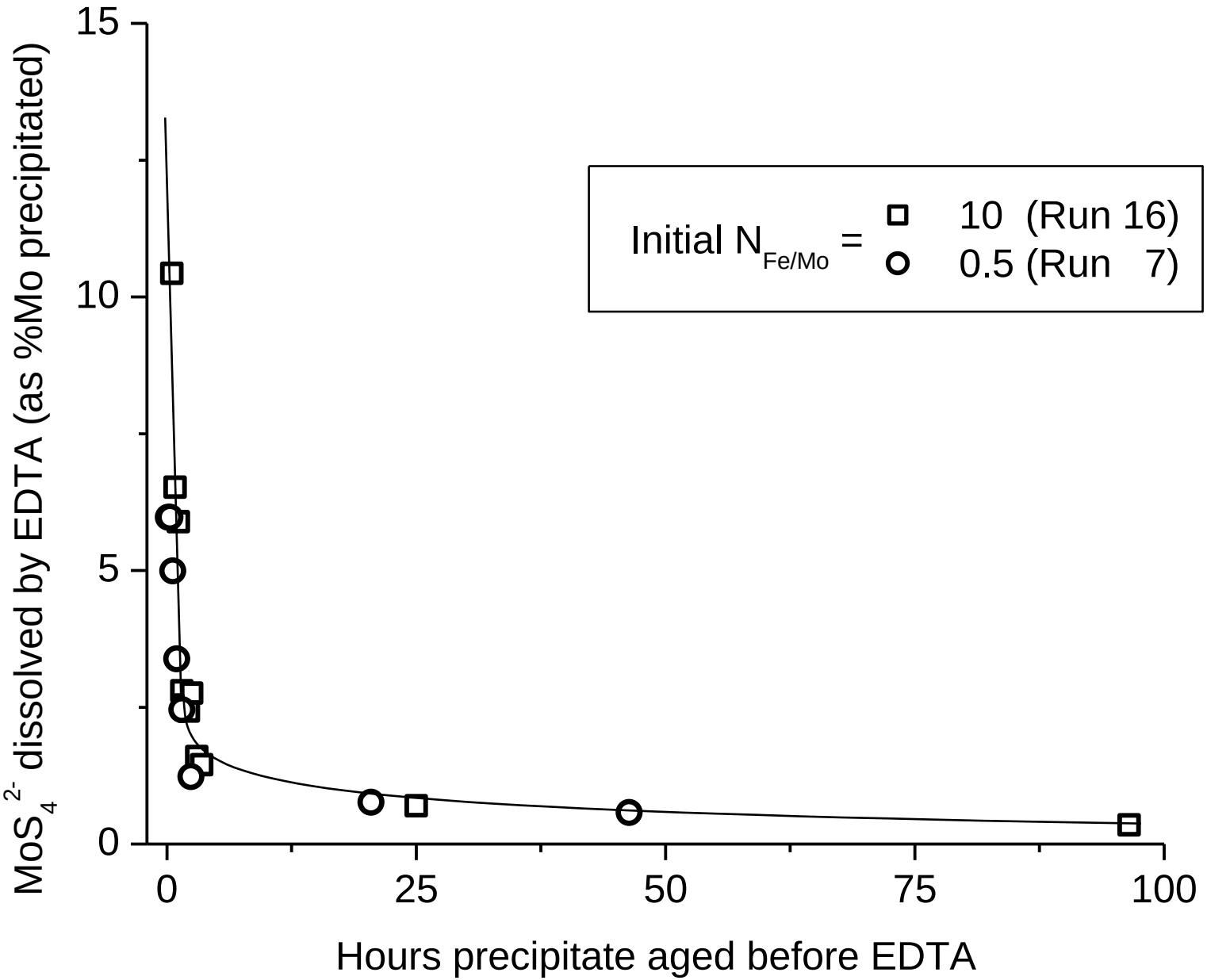
15
10
5
0
0
25
50
75
100
MoS4 2- dissolved by EDTA (as %Mo precipitated)
Hours precipitate aged before EDTA
Initial NFe/Mo =
10 (Run 16)
0.5 (Run 7)

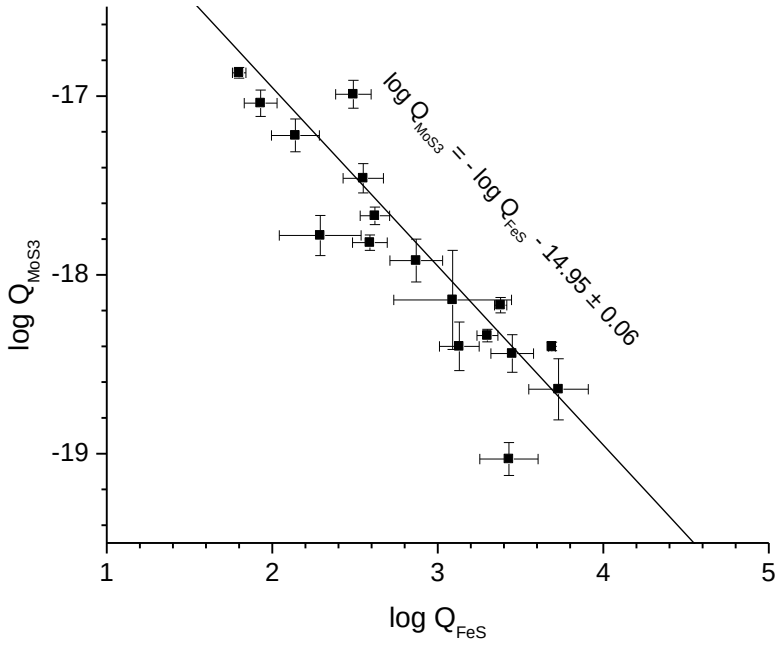

Figure 4

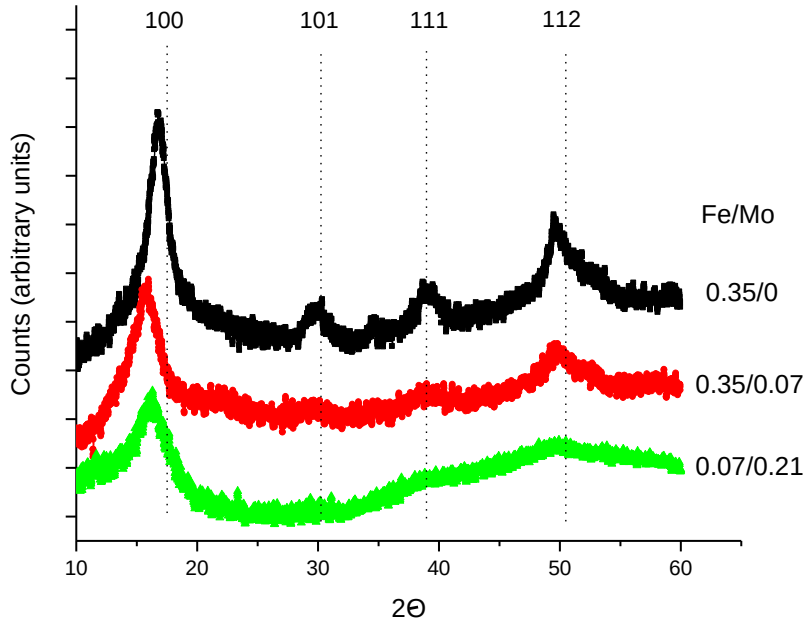
100
101
111
112
Counts (arbitrary units)
Fe/Mo
0.35/0
0.35/0.07
0.07/0.21
10
20
30
40
50
60
2Θ

Figure 5

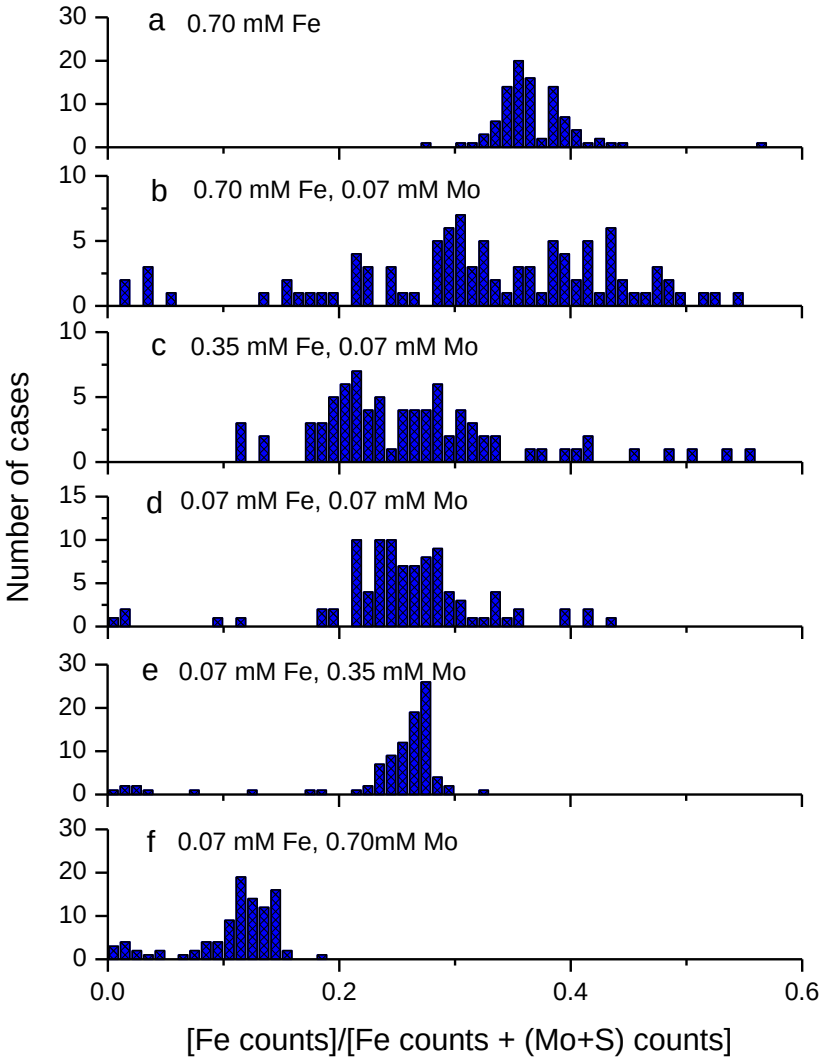
a 0.70 mM Fe
b 0.70 mM Fe, 0.07 mM Mo
c 0.35 mM Fe, 0.07 mM Mo
d 0.07 mM Fe, 0.07 mM Mo
e 0.07 mM Fe, 0.35 mM Mo
f 0.07 mM Fe, 0.70mM Mo
Number of cases
[Fe counts]/[Fe counts + (Mo+S) counts]

Figure 6

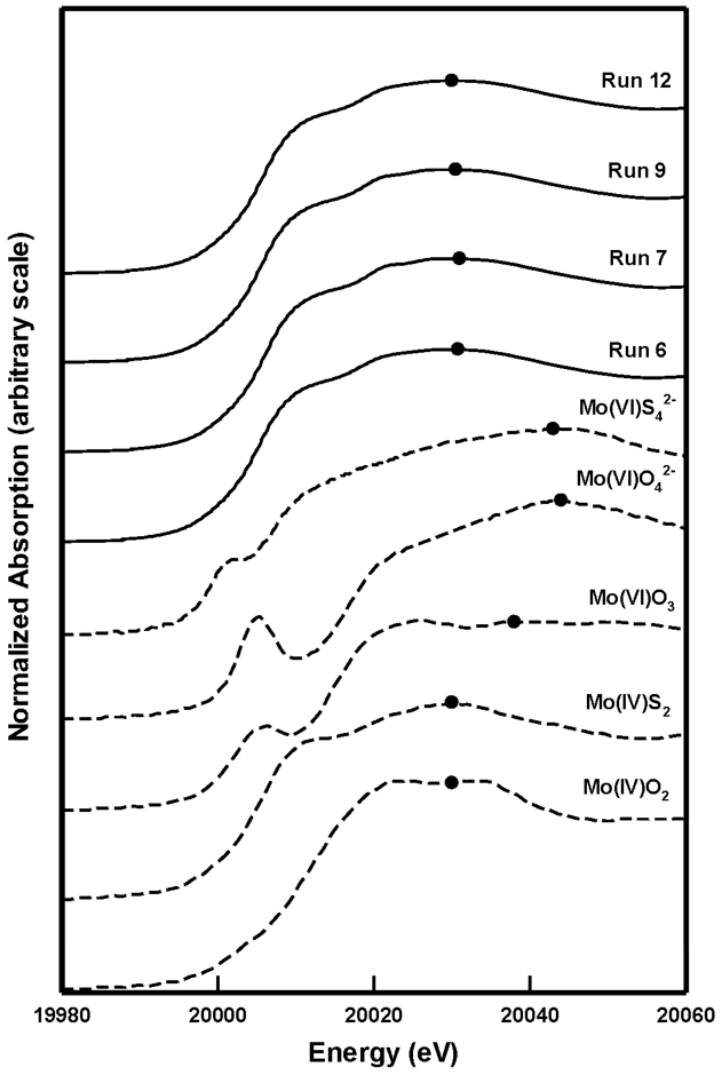
Run 12
Run 9
Run 7
Run 6
Mo(VI)S4 2-
Mo(VI)O4 2-
Mo(VI)O3
Mo(IV)S2
Mo(IV)O2
Normalized Absorption (arbitrary scale)
19980
20000
20020
20040
20060
Energy (eV)

Figure 7

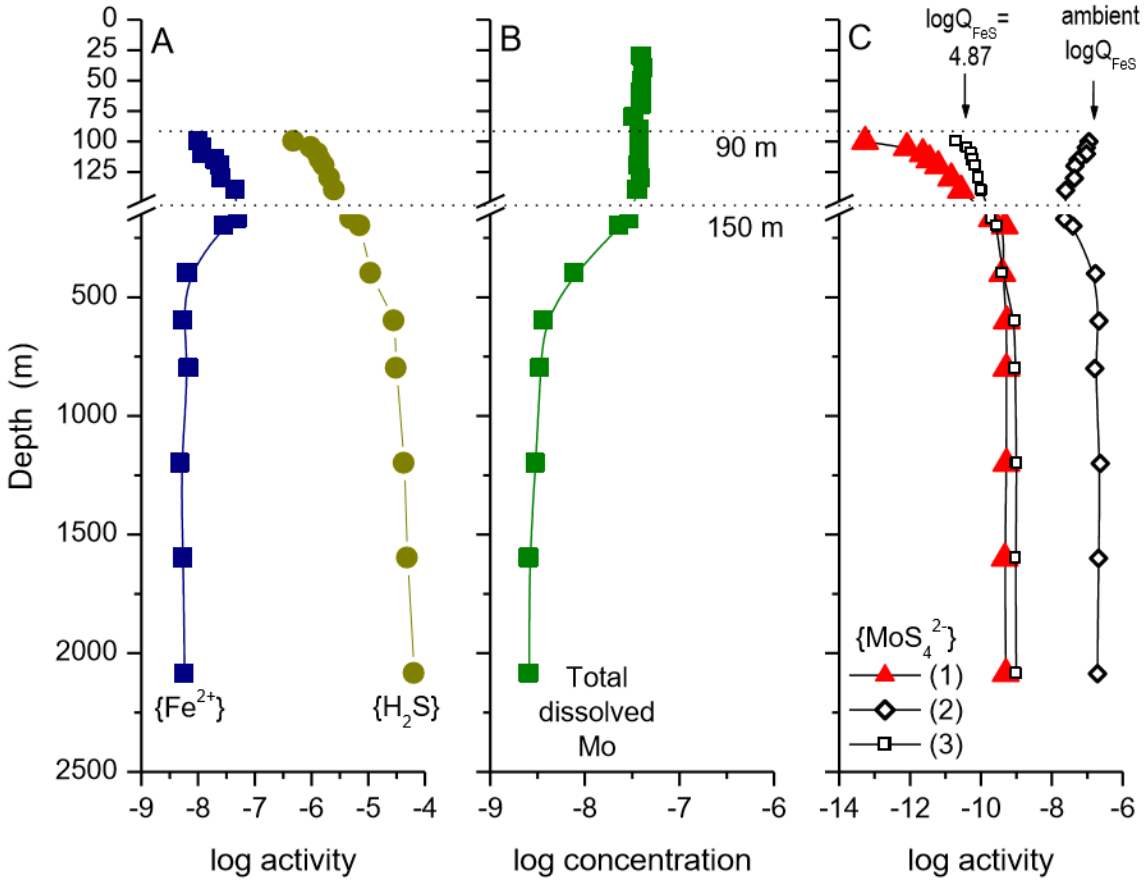
A
B
C
Depth (m)
0
25
50
75
100
125
500
1000
1500
2000
2500
90 m
150 m
{Fe2+}
{H2S}
Total dissolved Mo
logQFeS = 4.87
ambient logQFeS
{MoS4 2-}
(1)
(2)
(3)
-9 -8 -7 -6 -5 -4
log activity
-9 -8 -7 -6
log concentration
-14 -12 -10 -8 -6
log activity

Figure 8

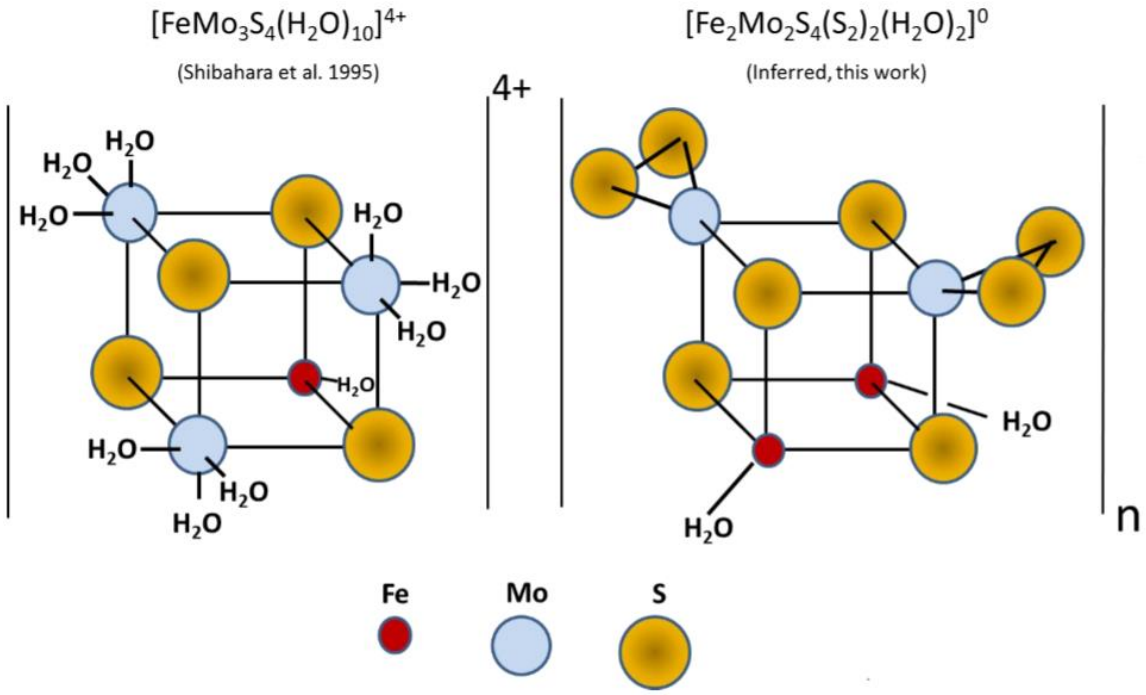
[FeMo3S4(H2O)10]4+
(Shibahara et al. 1995)
4+
[Fe2Mo2S4(S2)2(H2O)2]0
(Inferred, this work)
n
Fe
Mo
S

Figure 9

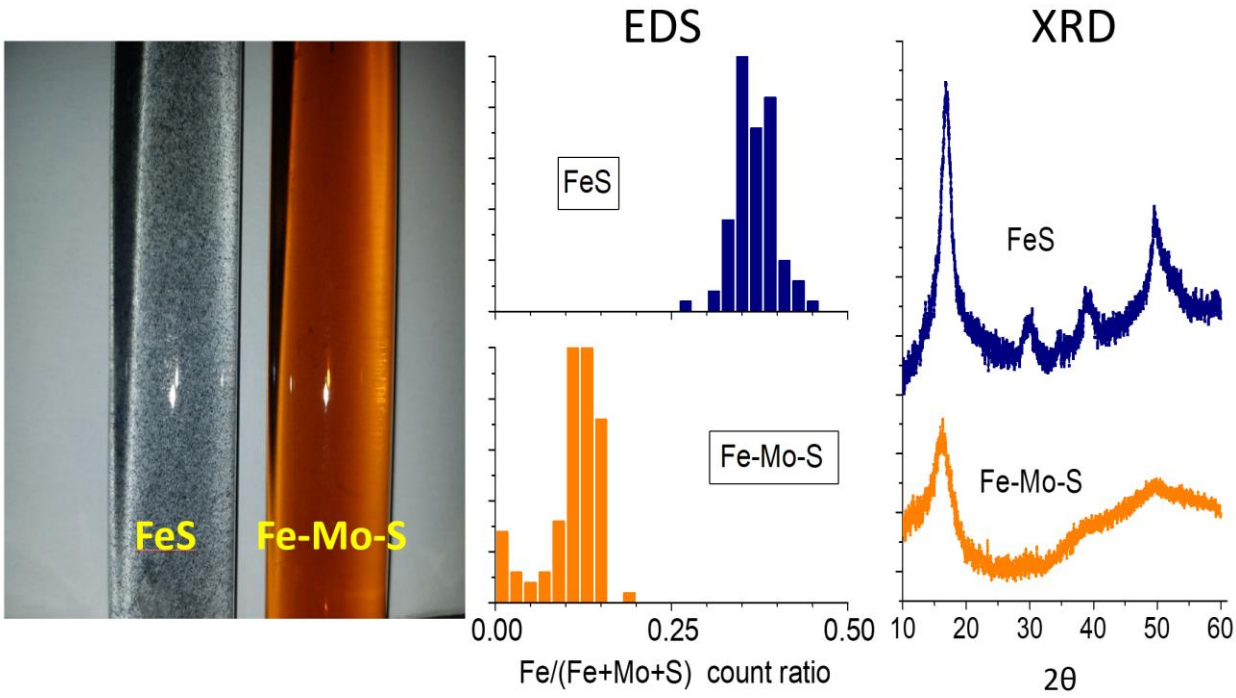
FeS
Fe-Mo-S
EDS
FeS
Fe-Mo-S
0.00
0.25
0.50
Fe/(Fe+Mo+S) count ratio
XRD
FeS
Fe-Mo-S
10
20
30
40
50
60
2θ

TOC Figure